Chapter 3
Interpretation of Geophysical Data for Regional Geology

3.1 Interpretation techniques for airborne geophysical data

Three different types of airborne geophysical data used in this study are in a grid-format with the same ground location or UTM grid reference. Each data set is manipulated and each output is treated differently depends upon their geological meanings.

3.1.1 Interpretation techniques for aeromagnetic data

The ideas on which the interpretation of magnetic contour maps are made and a more detailed discussion of some aspects of the work in the study are based on the works of Lidiak and others (1985) and Domzalski (1966). There are three parts of the interpretation: distinguishing the magnetic body by their intensity, determining shape and magnetic property of each body, and explaining the bodies in geological terms.

3.1.1.1 Intensity contrast

The simplest magnetic survey data interpretation is the use of intensity contrast. The total magnetic field coloured-contour maps or profiles were visually studied and qualitatively interpreted by comparing their intensities. Qualitative interpretations normally emphasize on structural mapping, magnetic zoning and geological features. Disruptions or deflections of trend in magnetic contour are always observed over faulting systems. Curvature and round-shaped contour may represent an intrusive body. The presence or absence of intrusive body is more important than its shape or its depth of buried in this sense. Magnetic zoning is reflected from the different magnetic bodies and their boundaries can be drawn. Each magnetic unit is characterized by its certain magnetic feature, intensity and relief.

In this study, it is essential to define the magnetic anomaly as the place where there is a considerable difference in magnetic intensity from the International Geomagnetic Reference Field (IGRF). It can be either positive (higher than the IGRF) or negative (lower than the IGRF) depending on the orientation of each magnetic body.

In Thailand, negative or much lower intensities from IGRF, between –20nT to –200nT, characterize magnetic anomalies. They are isolated or linear features with magnetic intensity decreasing toward the center. These were affected by the low magnetic latitude, or low inclination angle (Surinkum, 1990). It is known that magnetic map in low-magnetic latitudes of the northern hemispheres nearly always show a general pattern of negative anomalies on the north side. The expected ratios of amplitudes of positive and negative parts

approximately correspond with magnetic latitude, higher latitude greater positive amplitude (Grant, 1985b). Therefore, a pair of north negative and south positive, in this study area, is assigned as a magnetic anomaly.

The division of the magnetic contour map into a number of units is done to simplify the handling of the hundreds of individual anomalies of which the magnetic contour map is composed. Most anomalies can be included within the following five groups:

1. Circular bodies: These bodies may be more or less magnetic than the surrounding rocks. They are generally approximately circular or oval or pair of eclipses (Figure 3.1). The boundary limits are difficult to establish as the precise position of the boundary may be confused if the body is remanently magnetized. These circular bodies are very often due to intrusions of acid or basic plutons or volcanic necks. Small sedimentary basins will create a similar-shaped magnetic response. However, on a different scale, ore bodies may provide a circular pattern.

2. Simple sheets: Thin bodies usually, though not always, produce a single maximum and minimum (Figure 3.2). Simple sheets are the easiest to interpret. They are usually caused by a single, uniform magnetic body corresponds closely to the concept of the mathematical shape used in the calculations. The simple sheet may, on occasions, pass into a more complex band of anomalies and this may lead to minor confusion in the interpretation. Narrow linear anomalies may also be produced by faults and along the edges of very wide magnetic bodies.

3. Complex zones: They are a group of anomalies with broad magnetic zones (Figure 3.3). It is a convenient way to interpret complex zones at a first step because superimposed anomalies usually reflects on interesting magnetic map. The boundary may be clear in places, but the other side or the continuation along strike may become less distinct. Therefore the complex zone is usually open ended and often ill-defined. Wide areas of magnetic rocks that produce complex anomalies are often due to greenstone belts, bands of schist, thick iron formations, or intrusions of ultramafic rocks.

4. Dislocations: These changes in magnetic patterns indicate displacement of magnetic horizons in which case the dislocation is probably a fault (Figure 3.4). These dislocations may be marked by a change in the intensity or complete disappearance of magnetic anomalies along strike, or by the characteristic anomaly pattern of fault boundary. However, the term dislocation is preferred because it is related to a change in sedimentation, to an unconformity, to folding or to a fault. There are a number of situations in which the movement along the dislocation may be of the nature of a fault, but

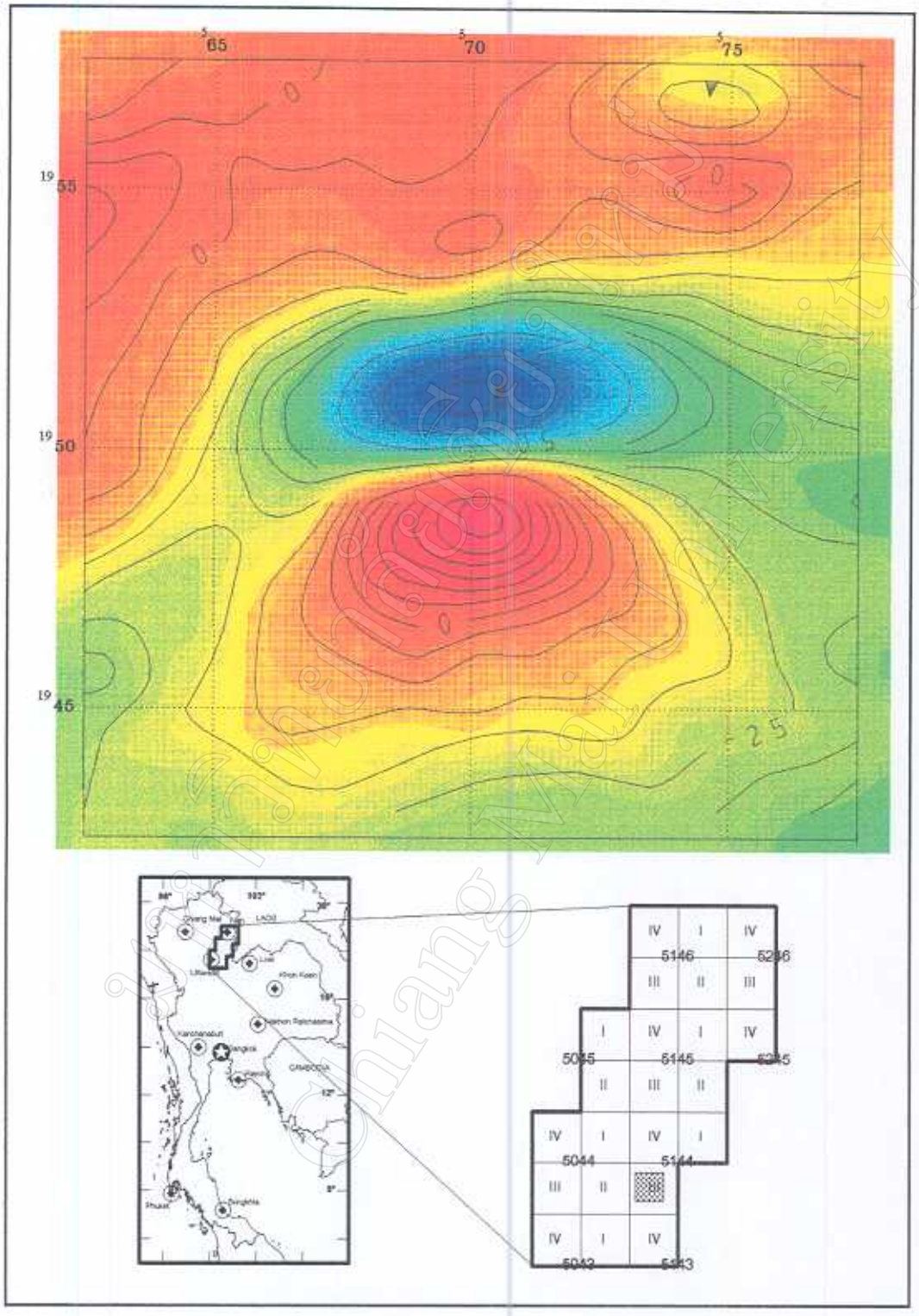

Figure 3.1 Aeromagnetic data showing a circular body anomaly.
(area covers negative value in the north and positive value in the south)

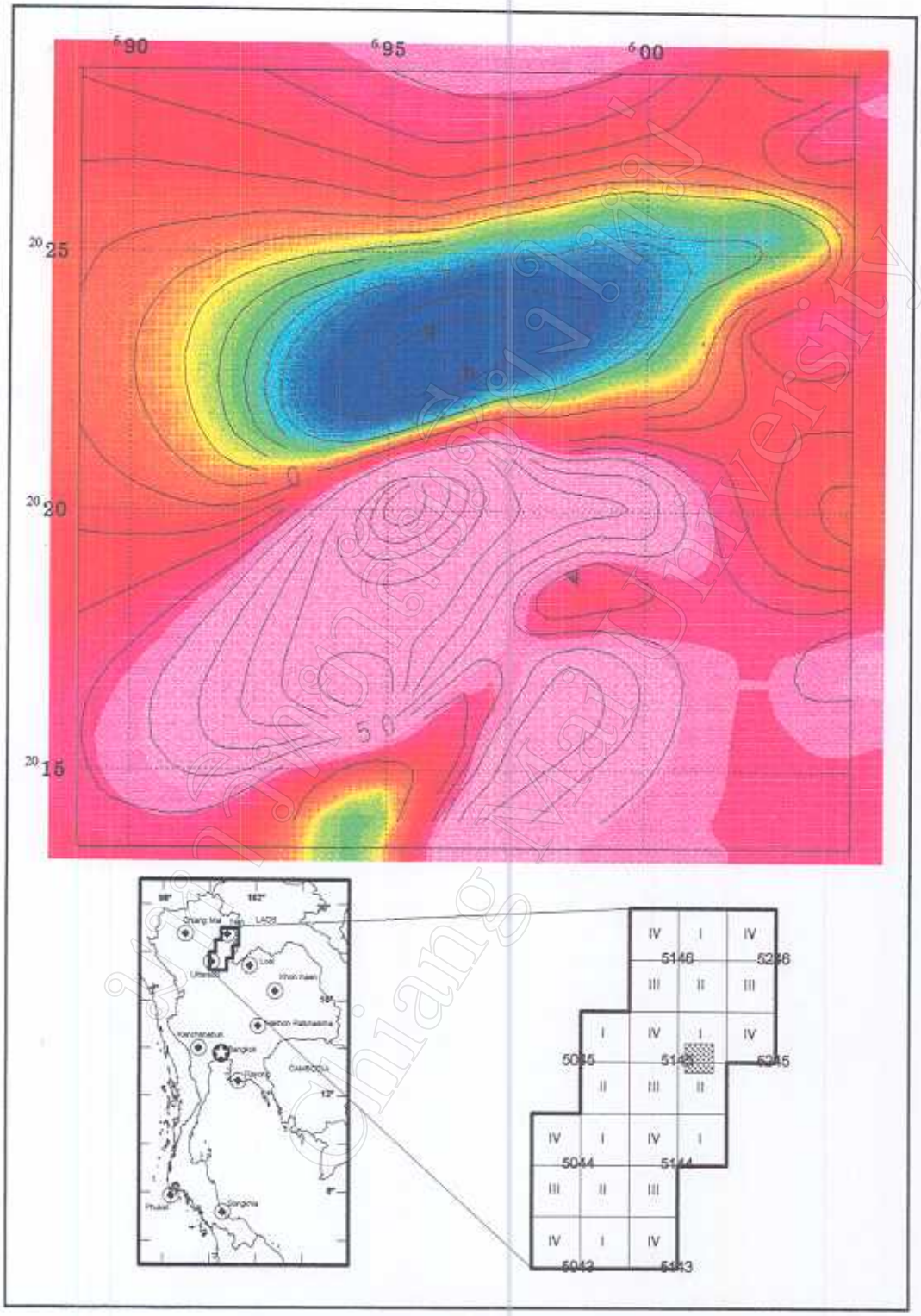

Figure 3.2 Aeromagnetic data showing a simple sheet anomaly.
(area covers negative value in the north and positive value in the south)

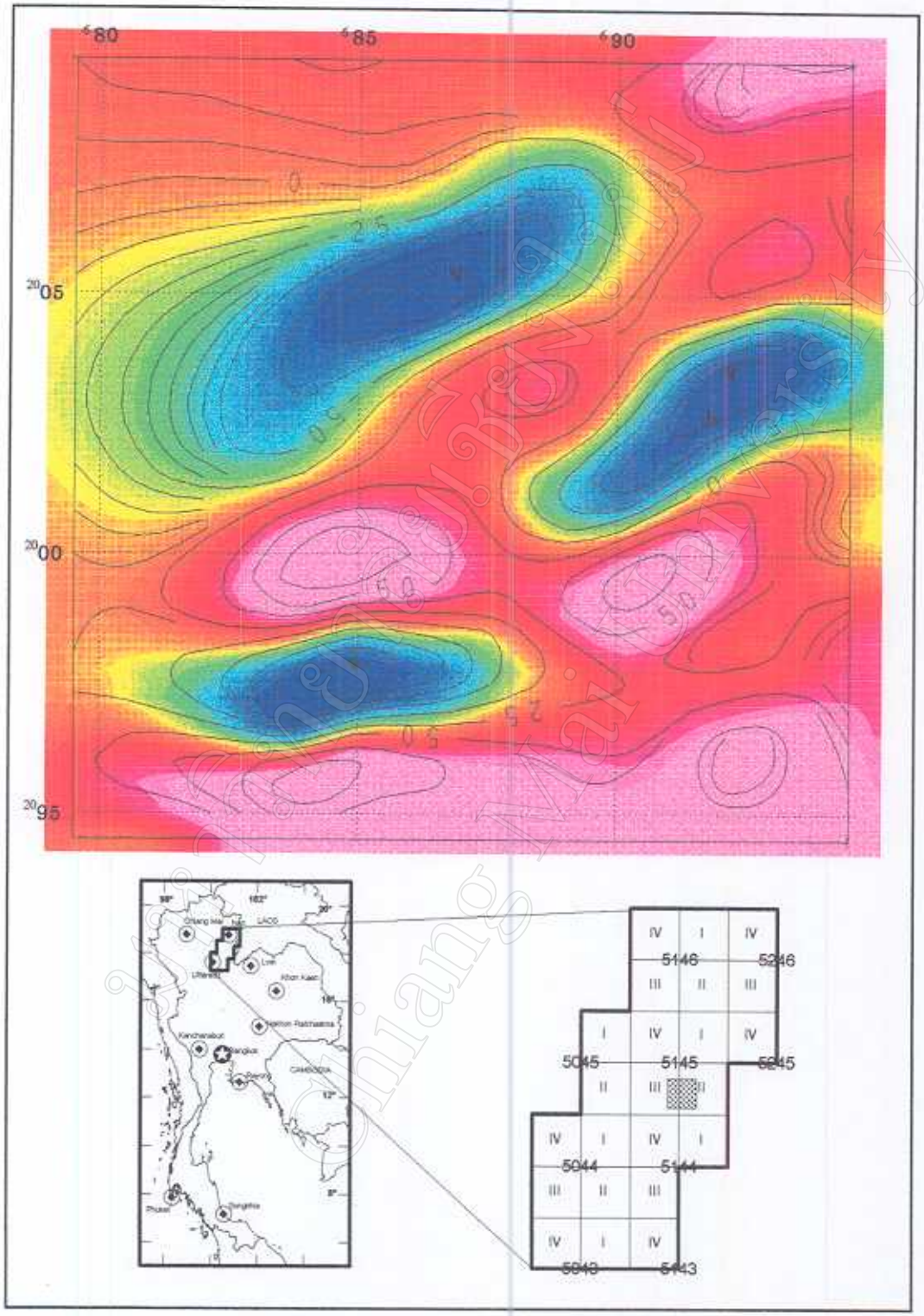

Figure 3.3 Aeromagnetic data showing a complex zone anomaly.
(area covers negative value in the north and positive value in the south)

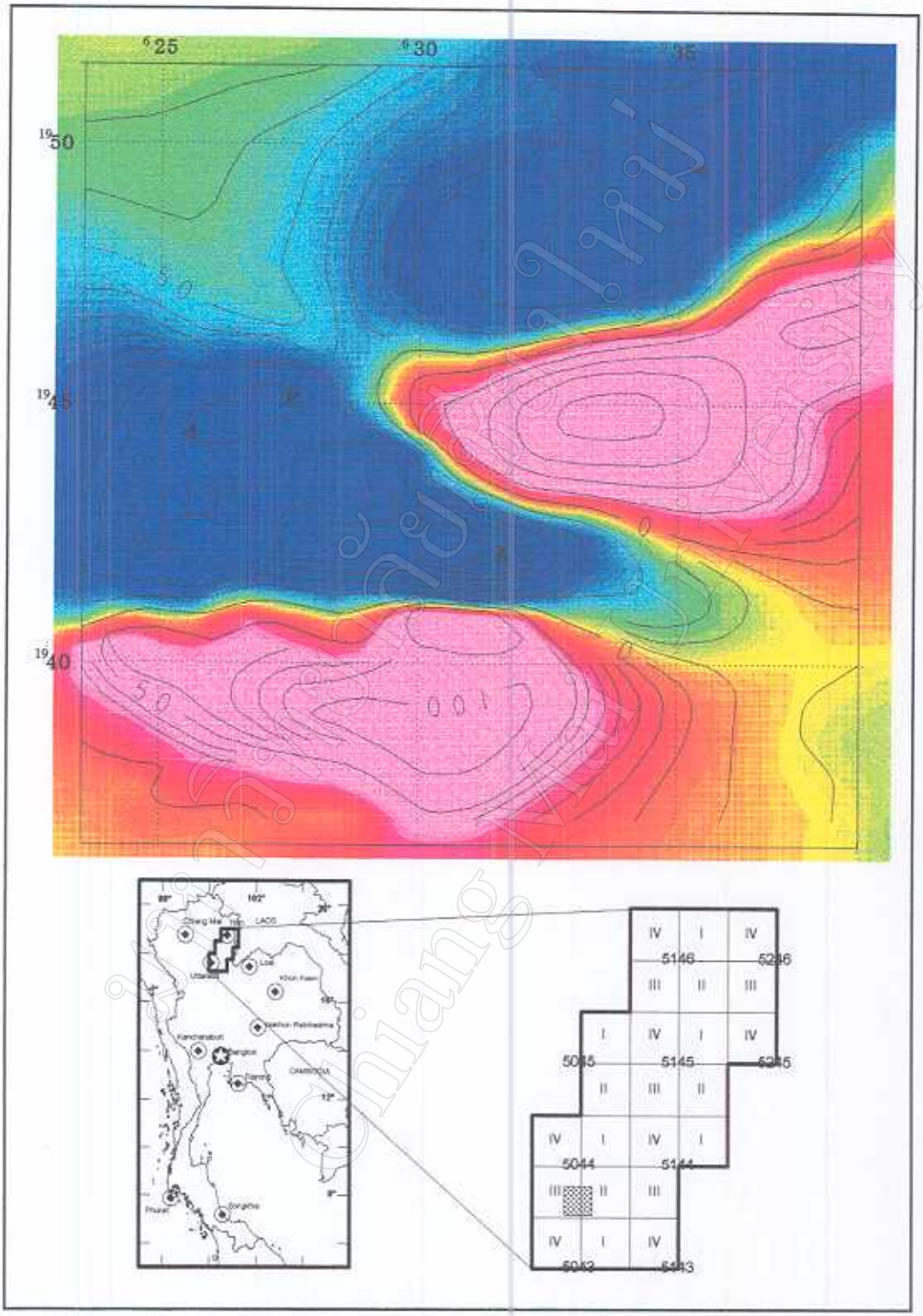

Figure 3.4 Aeromagnetic data showing a dislocation feature.
(area covers negative value in the north and positive value in the south)

does not necessarily take place within a limited volume, as is normally the case with a fault. There is also evidence of changes in the character of the sediments overlying large dislocations occur within the basement rocks. This may indicate that the faults were still moving during the period of deposition.

5. Superficial layers: These may be composed of either magnetic or non-magnetic materials (Figure 3.5). The magnetic layers are most likely to be basic lavas, but laterite might produce the same effect in very low-leveled surveys. On the other hand, magnetic blanket reduces the amplitude and increases the wavelength of the anomalies. Occasionally the sedimentary blanket is a magnetic layer.

A thin lens or a blanket of lava or sediments may form as overburden. The layer of lava can present a serious noise problem for the interpreter. However, the effect of the lava can be overcome in part by carrying out an upward continuation of data that will be mentioned later. It is often not too difficult to allow for the effect of the volcanics.

3.1.1.2 Time series analysis and enhancement

Apart from visual differentiation mentioned above, many enhance techniques can be applied to magnetic data in order to study a source of those anomalies. Each anomaly may not be generated from only one magnetic body but it is always a result of superimposed magnetic intensity from various sources. Those sources can be divided using mathematics approach, and digital signal processing, based on the potential field principles.

Robinson (1967) stated that two basic operations in digital signal processing are spectral analysis and digital filtering. One of the major events in digital processing was the work done by Cooley and Turkey (1965). They gave algorithms for computing the Fourier transform digital representation of the waveform. It became practical to manipulate waveform in computer in ways that would have been totally impractical with continuous representations. Moreover, the Fast Fourier Transform (FFT) algorithm assigned for discrete transform, summarized by Brigham (1974), was used as a more practical step for a digital signal processing. In general, applications of FFT are based on a specific implementation of discrete convolution or correlation integral.

Digital filtering has also been a major area of research in signal processing. In this method, a filter operator is designed for the data depending upon the solution of a set of equations. Except for short filters, the requirements for computer storage space and computer time for solving those equations by the use of standard simultaneous equation routine are prohibitive. So, the filtering done by FFT algorithm is being applied to all potential data set used in this study.

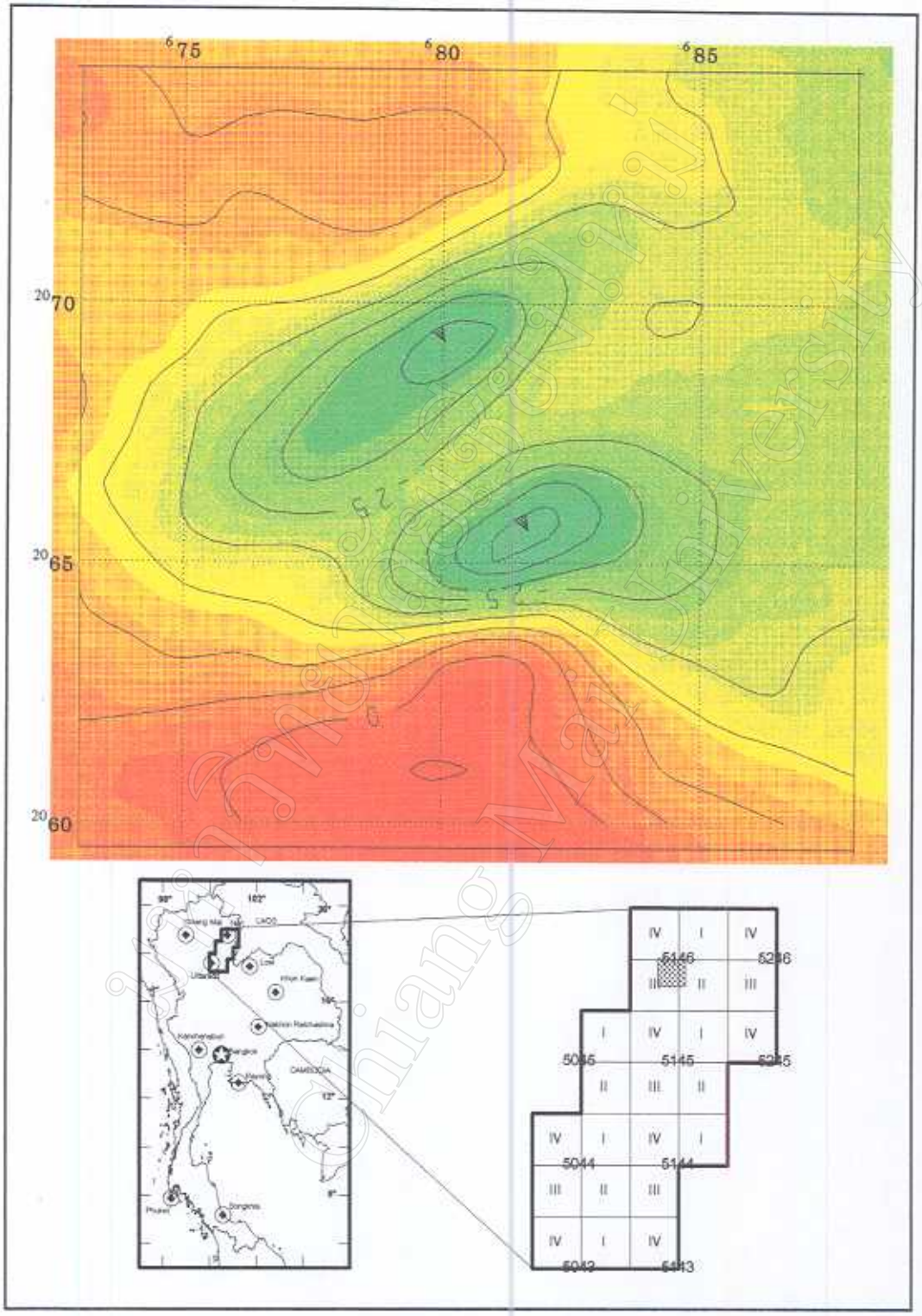

Figure 3.5 Aeromagnetic data showing a superficial layer.
(area covers negative value in the north and positive value in the south)

There are numbers of operation, which are facilitated by Fourier Transformation, including the followings: spectrum analysis, upward continuation, shading and analytical signal. These operations are used to resolve anomalies of deep origin, reconstruct a body at depth and define a body in areas of low magnetic inclination like Thailand.

Spector and Bhattacharyya (1966) showed that spectral analysis is useful for interpreting magnetic field results. They used energy density spectrum and autocorrelation function to define a simple magnetic body successfully. Surinkum (1989) applied two-dimensional Fourier transform to determine the depth of the regional structures in Sa Kaeo suture zone. The north-south trending equatorial structures, usually show no magnetic anomaly, can be outlined by analytical signal filtering (Beard, 2000).

In order to study the regional geology of this study area, a number of enhanced techniques were applied. First, the data over the study area were gridded from combined data from Survey A and HEM survey with 500X500m interval and with the sensor at 500m mean clearance. Gridded data shown in Figure 2.2 was used as a correlation base map. The first group is an upward continuation result where magnetic sensor is assumed to level up from 500m (Figure 3.6a) to 1000m (Figure 3.6b), and 2500m (Figure 3.6c) and 5000m (Figure 3.6d), respectively. The technique simply shows that the sensor has more effects from the shallow magnetic body at a lower altitude whereas that at the higher altitude has more effects from the deeper one.

In this study area, the magnetic anomalous zone can be divided into five different zones characterized by the above criteria. They include high magnetic zone (HZ) characterized by high magnetic intensity located in the middle of the study area (Figure 3.6a). This zone is composed of complex zones and dislocations. They can be related to areas of the ultramafic unit. A lesser magnetic or medium intensity zone (MZ), both south (MZ-1) and north (MZ-2) of the HZ, is composed of simple sheets. In the south, there is one circular body (CB-1) of high magnetic intensity located within the MZ-2. Apart from these zones, there are two low magnetic intensity zones (LZ). LZ-1 in the south can be related directly to a sedimentary sequences of Jurassic (J) and Cretaceous (K) (Figure 1.7). Two circular bodies of medium magnetic intensity, CB-2 and CB-3 are found within the area of LZ-2 (Figure 3.6a).

Enhanced results show that this area can be divided into three different parts. Tectonically, this area is composed of three terrains, low magnetic in the southeast, high magnetic in the middle, and moderate magnetic in the northwest (Figure 3.6d). It can be seen that these three terrains can be referred to an area of redbeds, a complex zone, and sedimentary sequences with igneous activities, from southeast to northwest, respectively.

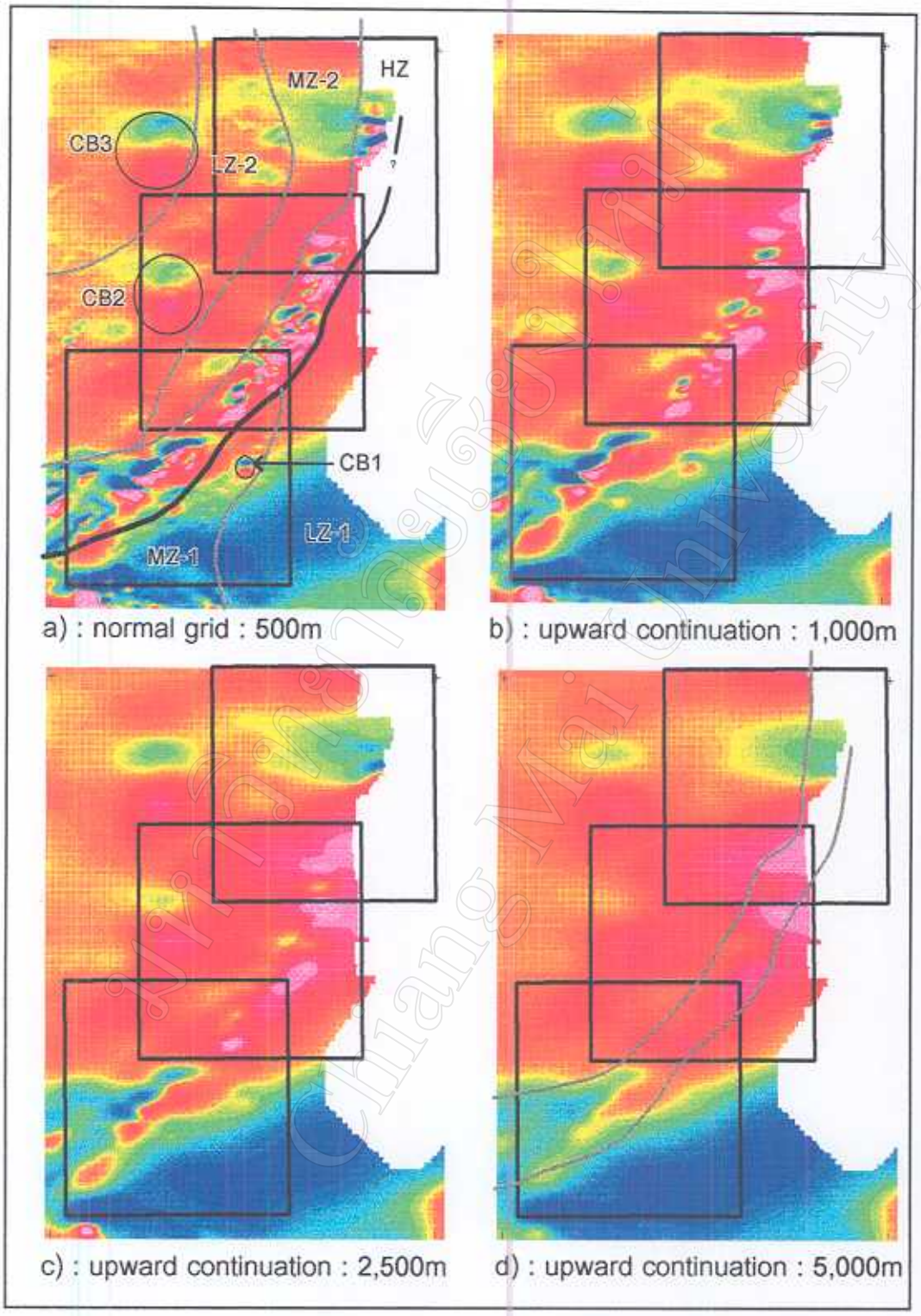

Figure 3.6 Aeromagnetic data enhanced by upward continuation.
(scale referred to Figure 2.2)

Other enhanced applications: analytical signal, x-derivative and shading, are shown in Figure 3.7. Analytical signal technique was applied to the normal grid data (Figure 3.7a) in order to outline the source of the magnetic anomalous zone (Figure 3.7b). This technique is used in complex trace analysis by determining the phase of a minimum function. This analytical signal is then used in computing a deconvolution operator. In this study, deconvolution with x-derivative was selected to enhance the direction of the magnetic body whose intensity is higher than the surroundings (Figure 3.7c). Shading technique was also applied to the data in order to compare the enhancing results (Figure 3.7d). Shading result shows that the magnetic anomalous zones in this area are not continuous zones and each can be separated with confined outlines. Although their axes are lined in different directions, they tend to be in a northeast-southwest direction.

When an analytical signal of the northern part (Figure 3.8) is correlated to geological data, many distinct features are outlined. To the northeast, magnetic sources connect to each other at depth. Their intensities indicate that sources are from ultramafic unit mapped as U units. These two U units should lie underneath the Permo-Carboniferous (CP) unit in the west and Jurassic (J) unit in the east. To the west, isolated magnetic sources lying in a north-south direction may represent volcanic sources of Mesozoic volcanic (Mzv) units. The center of each isolated anomaly may indicate where the volcanic rock extruded. There is a group of high magnetic intensities in the south, where geological data indicates a small outcropping of the U unit. This shows that the U unit may extend wider than it was mapped and this group of high magnetic intensities cannot be reflected from a single U unit. These suggest that the northern part can be divided, from west to east, into three parts: volcanic zone, fold belt, and ultramafic zone. The red bed units, J units, shown in the geological map cannot be explained by this analytical signal because of the limitation of the survey data.

Analytical signal over the central part can be partly correlated with the mappable rock units (Figure 3.9). The U units correlate very well with the analytical signal even though the signal reflected more units than the mapped units. It also shows that the U unit extends toward the reservoir and projected underneath the Carboniferous (C) and Silurian-Devonian (SD) units to the south. To the west, the analytical signal shows that there should be some volcanic units correlating with the Mzv mentioned earlier.

To the south of the reservoir, W area, the magnetic sources equivalent to the U unit sources extend southwestward. Its extension can be traced southward underneath the Quaternary alluvium (Qa) and Quaternary terrace (Qt) units (Figure 3.10). The U unit in this area is the parent of lateritic layers

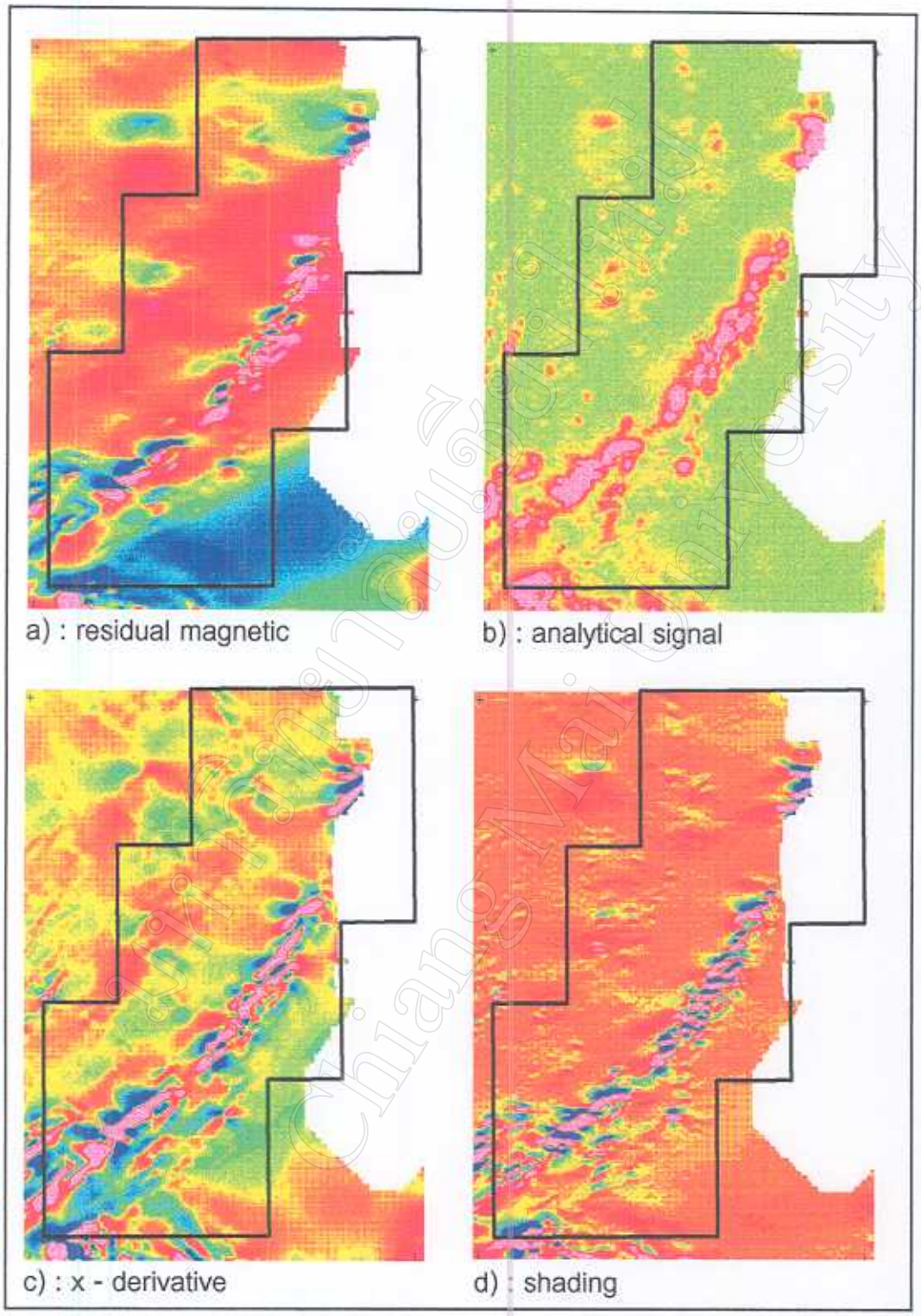

Figure 3.7 Aeromagnetic data enhanced by various techniques.
(scale referred to Figure 2.2)

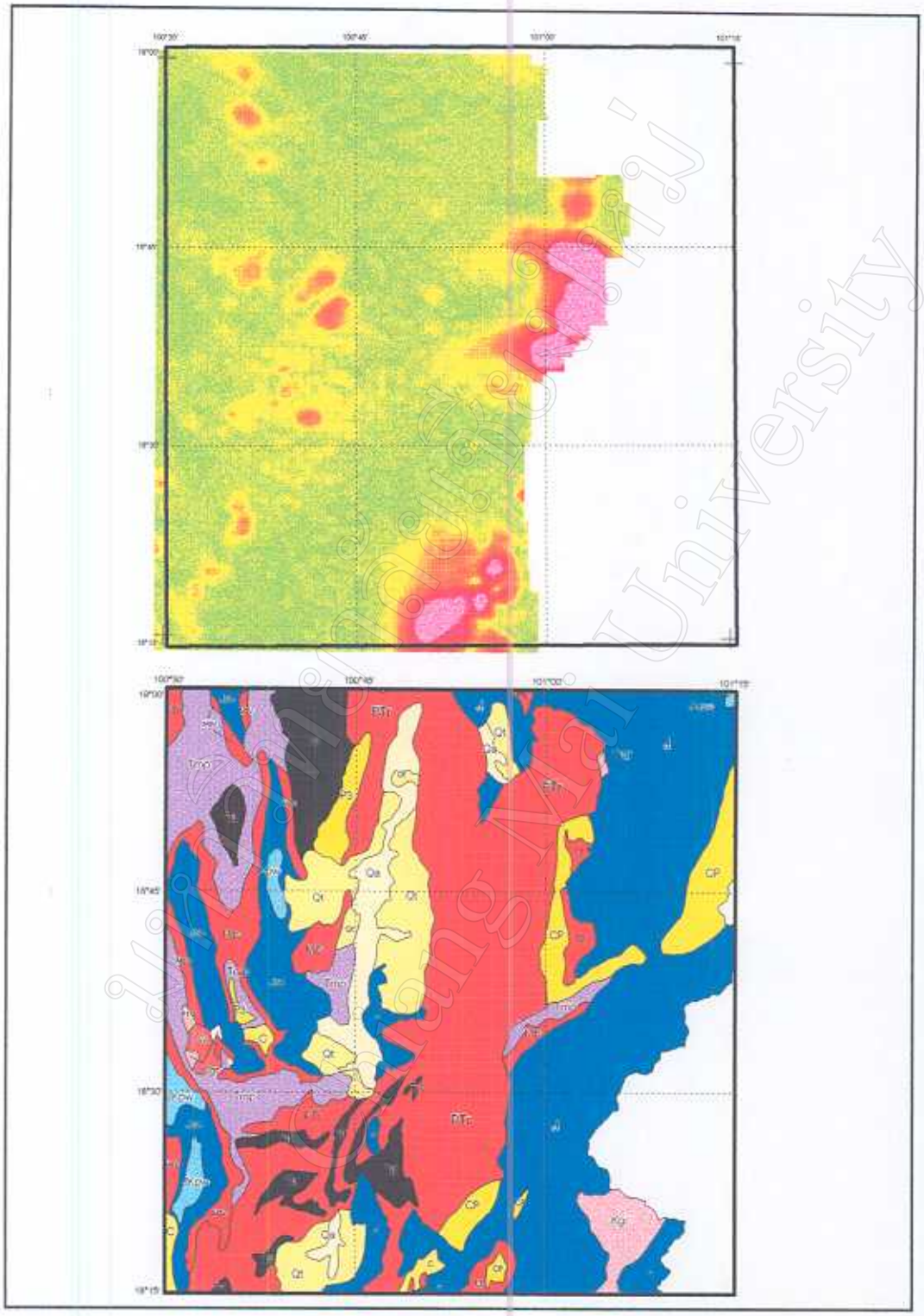

Figure 3.8 Correlation of analytical signal of aeromagnetic data and geological map of the northern part.
(symbols are the same as those in Figure 1.5)

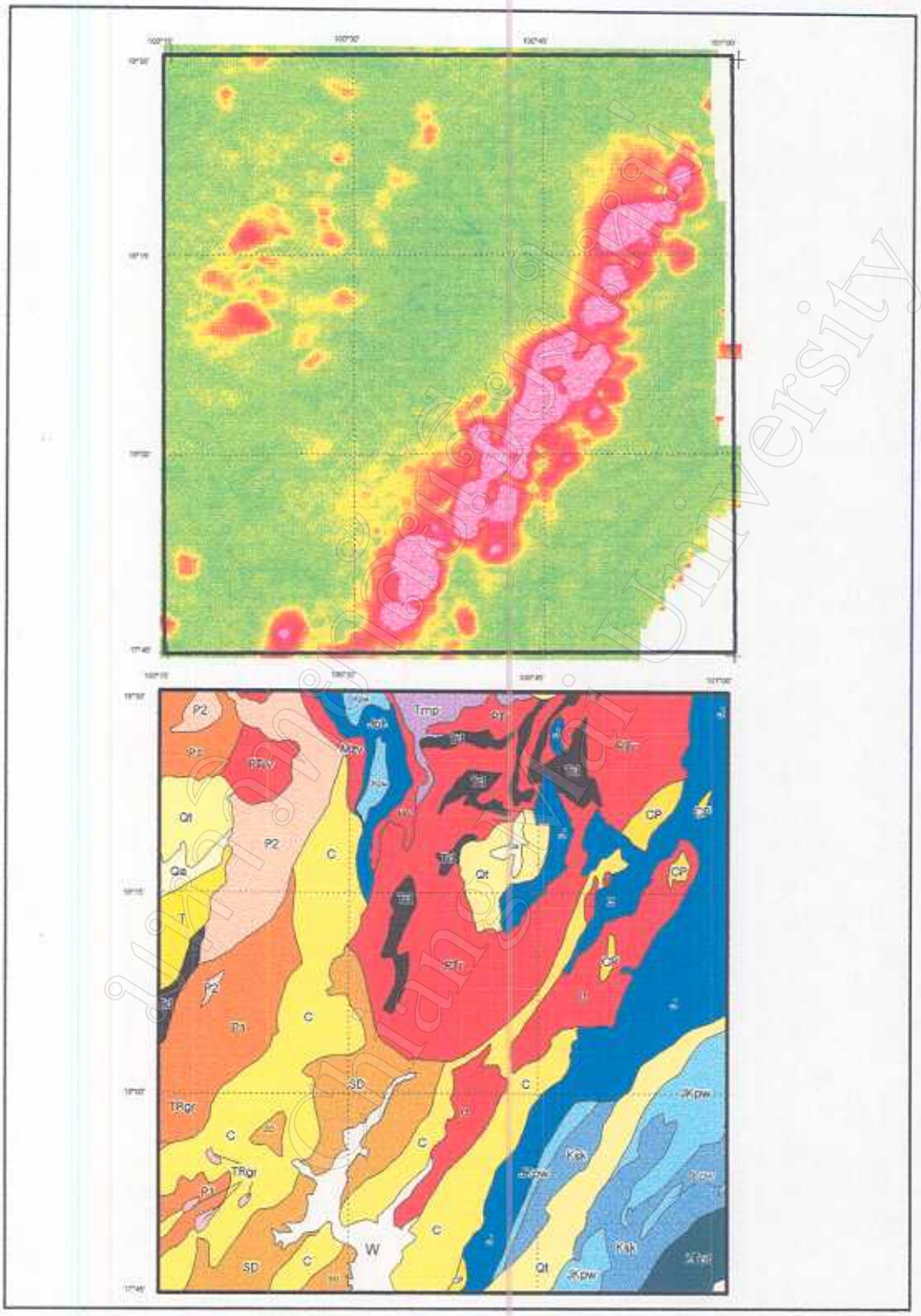

Figure 3.9 Correlation of analytical signal of aeromagnetic data and geological map of the central part.
(symbols are the same as those in Figure 1.6)

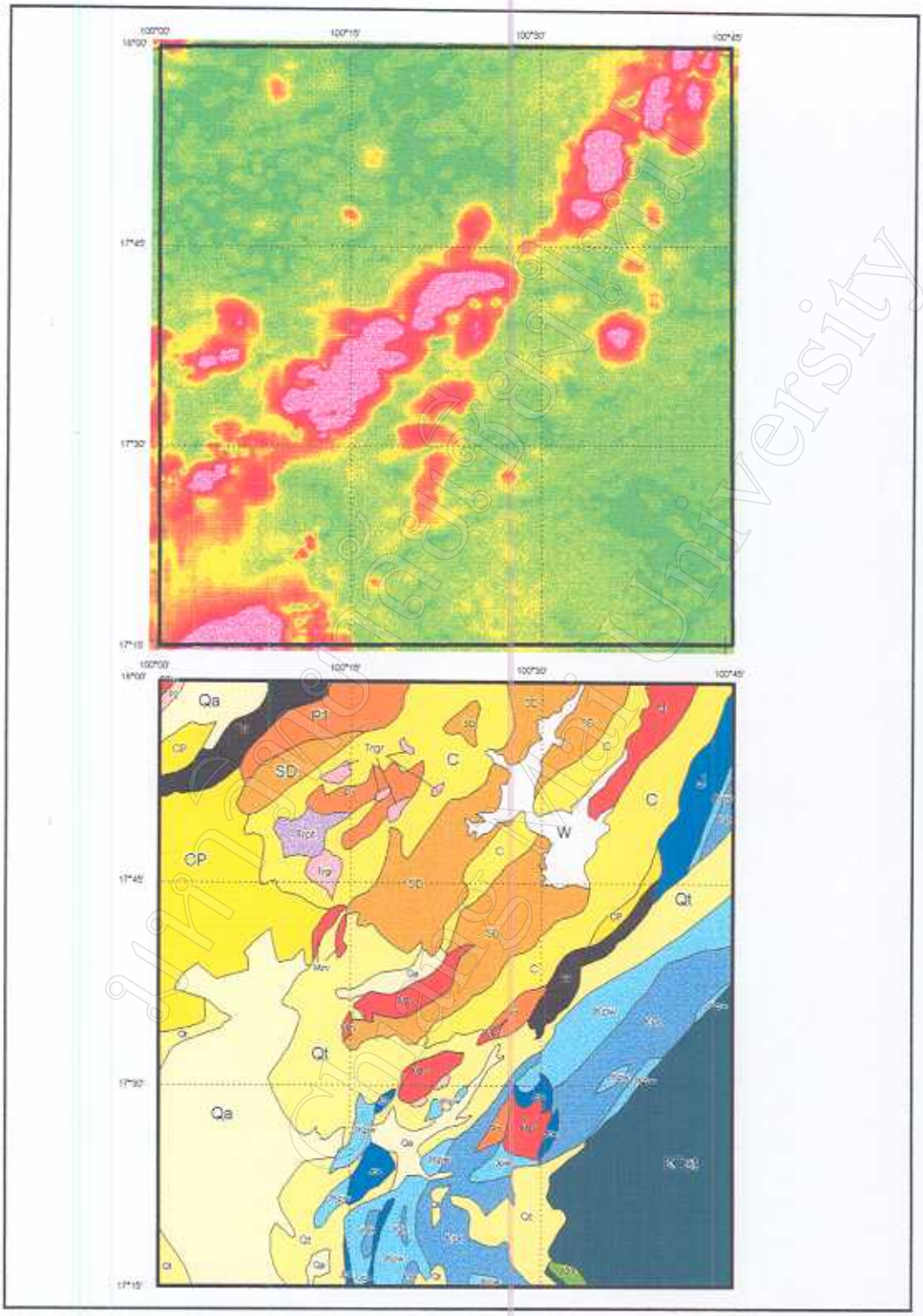

Figure 3.10 Correlation of analytical signal of aeromagnetic data and geological map of the southern part.
(symbols are the same as those in Figure 1.7)

with nickel-chrome iron found in Phra Than Dong Rung temple reported by Buravas (1941). Analytical signal of this southern part also shows that a circular analytical signal in the east cannot be correlated to the mapped unit. This circular signal may be reflected from some intrusive bodies without any exposure. The only surface signature related to intrusive activity is lateritic soil formation, formed by weathering process. On the other hand, the Mzv unit mapped in the south may be less spreading than it was shown in the geological map and the Mzv unit in the west should be more acidic than the southern one because it was magnetized to a lesser degree.

3.1.1.3 Modelling

It is convenient to pre-calculate the response of simple bodies, which may be expected within the area of study. The responses of thin sheets, which strike east-west, north-west and north-south, and dips through the range of 30, 60 and 90 degrees in both directions, are usually enough. It is also useful to have one or two models for vertical prisms, which are roughly equidimensional. In the areas of low magnetic latitude, it is convenient to have a number of models for thin prisms which strike north-south. The information is readily available in works published by Vacquier and others (1951), Reford and Sumner (1964), and Grant and West (1965).

Prior to fitting geological models, each selected profile was plotted to common scale in order to compare the anomaly intensities. Some profiles contained more than one causative body in a geological model. Each geological model due to each magnetic anomaly will be separately examined but interpreted as a continuous structure. In this study area, five profiles, two north-south trending profiles and three northwest-southeast trending profiles, are proposed for modelling (Figure 3.11).

Line A, Line C and Line D are lines selected for disclosure and complex zones where Line E is for circular bodies. Line B is laid over both complex zone and a circular body. Once the profile is selected a basic geologic cross-section of each line is inferred from the existing information or from correlated information nearby. The realistic starting model, based on geology rather than geophysics, is necessary because of the well-known problem of ambiguities in interpretation of potential field data which, without appropriate constraints, can lead to an infinite number of combination of body geometries and magnetic properties producing any given anomaly.

Normally, it is necessary to define more than one causative body into the modelling procedure. A simple causative body can be defined from each anomalous zone, a distinct magnetic field strength different from the IGRF analyzed by vector analysis (Surinkum, 1989). A magnetic profile over each

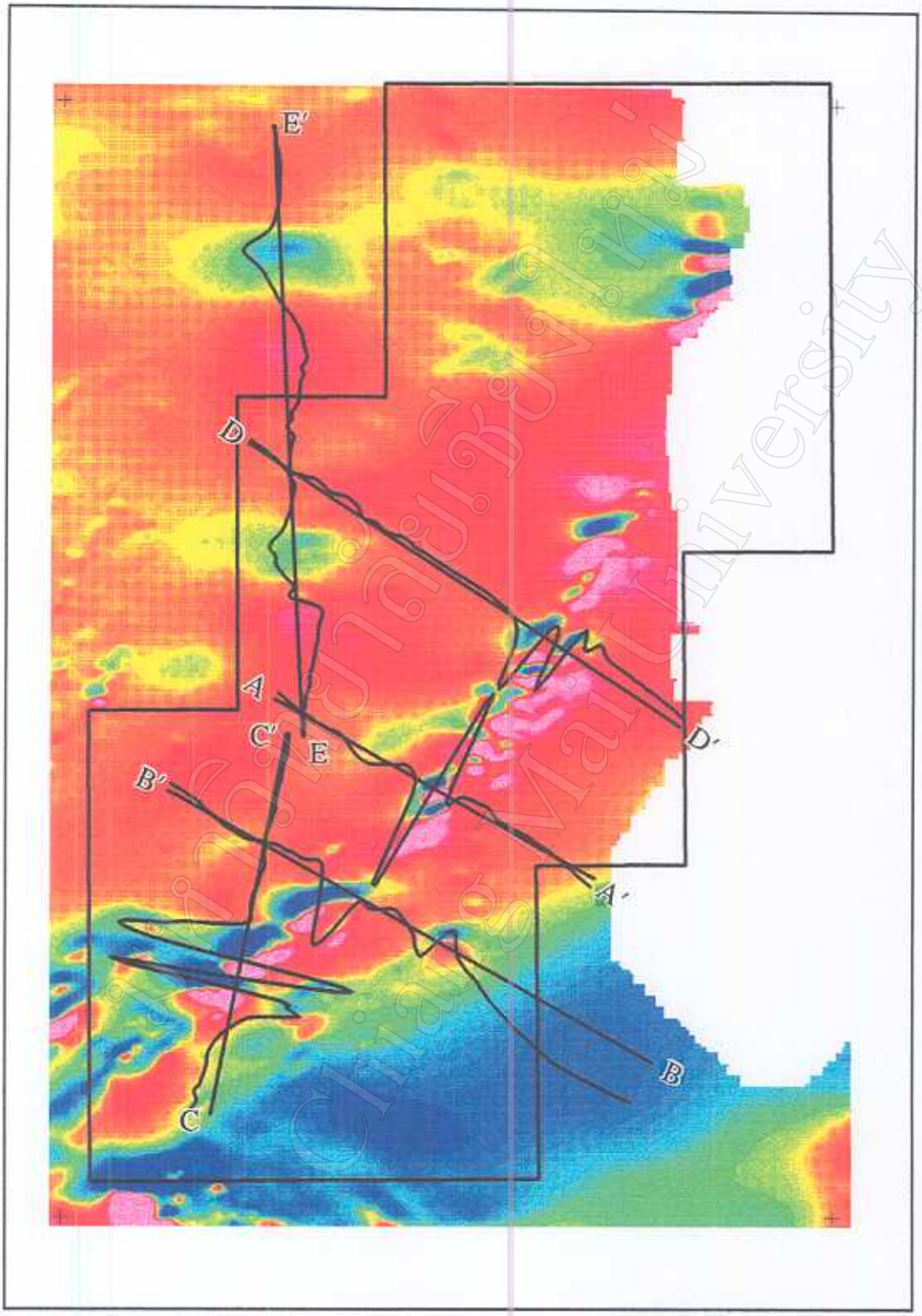

Figure 3.11 Map showing the five proposed aeromagnetic modelling profiles.

anomalous zone will be examined, from south to north, according to the potential field theory (Hjelt, 1976). Some definitions of causative body buried in the low magnetic latitude like northern Thailand are:

Wide negative anomaly appearing as tilted trapezoid shape (Figure 3.12a) will reflect an intrusive structure. The trapezoid declines toward the lower negative anomaly side. The intrusive body will not be wider than the longest side of the trapezoid.

A tabular structure will be reflected by a major negative anomaly appearing as asymmetric U-shaped (Figure 3.12b). The south side (left-hand) shows steep slope compared to gentle slope of the north side (right-hand). Center of the tabular body will be located within 1/4 to 1/3 from the bottom of the U toward the south side (steeper slope). The tabular body, therefore, will not be greater than the left half (south side) of the U-shaped.

A major negative anomaly appearing as an upside down bell-shaped will reflect a small normal fault with a north side downward (Figure 3.12c). The north side downward shows steep slope at the north side (right-handed) whereas the south side shows gentler slope. Fault body should be located at approximately 1/4 to 1/3 from the bottom of the bell toward the north (right-handed).

A big normal fault with a south side downward will also be reflected by positive anomaly as big bell-shaped (Figure 3.12d). The south side (left-handed) of the bell gently declines toward the south direction, whereas the north side (right-handed) declines steeper toward the north. Fault body will be located at approximately 1/4 to 1/3 from the top of the bell toward the north side, which is moving upward.

A big normal fault with a north side downward will also be reflected by negative anomaly as big bell-shaped (Figure 3.12e). The north section shows steep slope compared with gentle slope of the south side. Fault body will be located at approximately the bottom of the bell to 1/4 of the steep slope toward the north, which is moving downward.

A major positive anomaly appearing as bell-shaped will reflect a small normal fault with a south side downward (Figure 3.12f). The south side downward shows positive anomaly while the north side upward shows negative anomaly. At the top, the bell declines a little toward the north (right-handed side). The fault body will be located at approximately ¼ to ½ from the top of the bell toward the northern side.

A major negative anomaly appearing as V shaped (Figure 3.12g) will show a dike-liked structure. The left-handed side represents a south direction whereas the right-hand side represents north. The center of the body is located

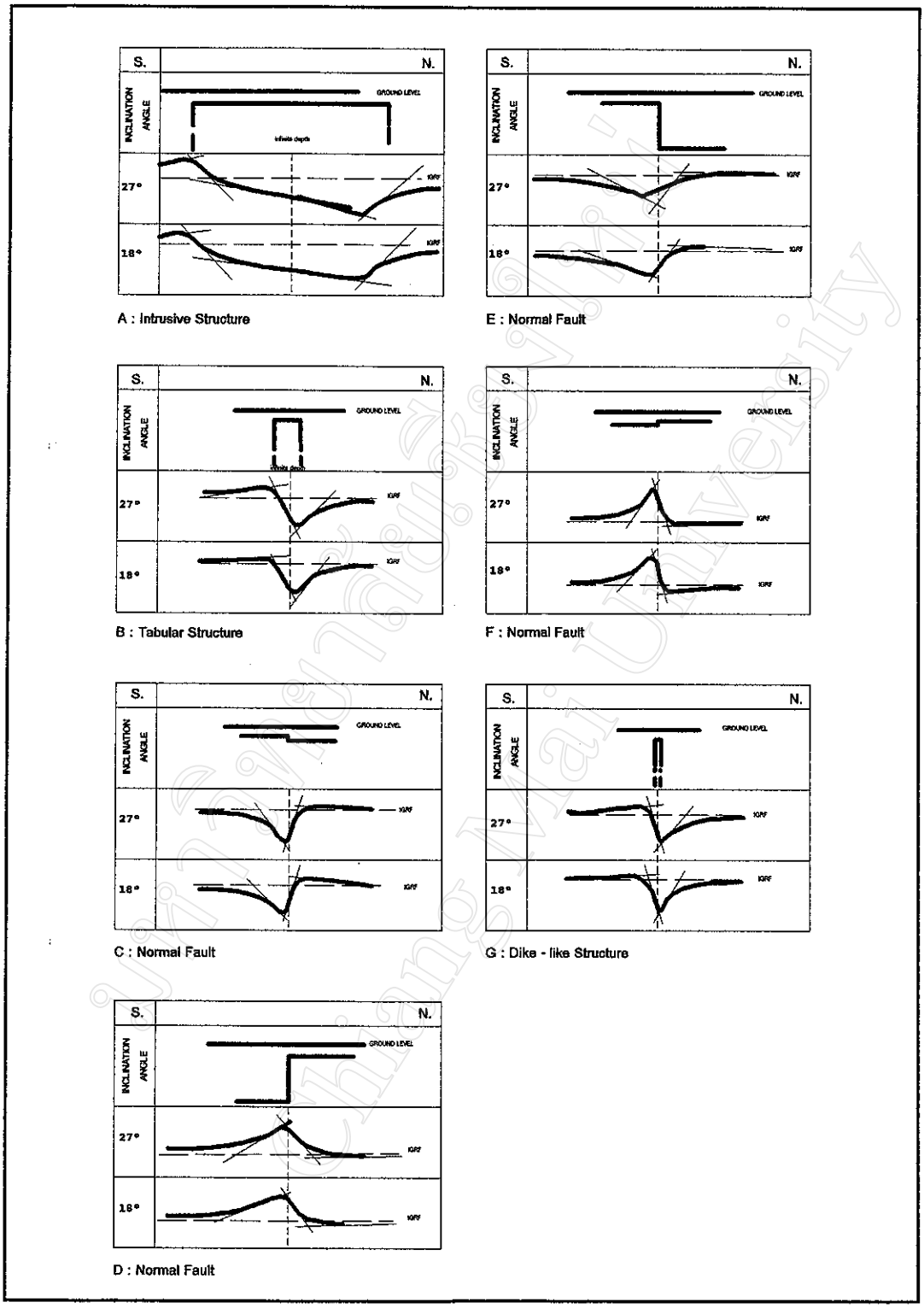

Figure 3.12 Anomalous magnetic profiles over a simple magnetic body.

at approximately 1/3 of the highest gradient (left-handed slope) on the south side. The body, therefore, will not be wider than the south side (left-handed slope of the V) of the highest gradient.

The modelling results of each line are shown in Figure 3.13 to Figure 3.21. In order to compare all causative body orientations, a tabular model type is selected to represent them all. Each modelling result, magnetic profiles, observed or measured, and fitted or calculated, is plotted in the upper section. The lower section is the model representing the calculated profile. The orientation of the model is presented as a magnetic body laid perpendicular to the selected profile and inclined toward the strike of each line. The model parameters are listed with the profile. It should be noted that all are best fitted and each parameter is used to explain different magnetic causative bodies. The scales of both sections are set according to the profile and model parameters.

In the central part of the study area, Line A is laid out over two magnetic anomalies. The magnetic body in the west is dipping toward the northwest, 162 degree clockwise or 18 degree anti-clockwise when compare to the strike of the profile (Figure 3.13). Its magnetic susceptibility is high (0.0191 emu). To the east of Line A, a lesser magnetic intensity is reflected from a lower magnetic susceptibility body with 0.0167 emu, and a similar dipping but different extension (Figure 3.14).

The magnetic anomalies in Line B are similar to Line A but with less intensities, -250 nT compared to -350 nT (Figure 3.11). Modelling in Line B starts from southeast toward northwest, opposite to Line A in order to compare the result of both lines (Figure 3.15 and Figure 3.16). The result shows that the magnetic bodies are dipping toward the same northwest direction. The model in the west part of Line B (Figure 3.15) has a higher magnetic susceptibility whose body is buried shallower than the east one (Figure 3.16). The one west of Line B (Figure 3.15) is similar to the one west of line A (Figure 3.13) in both orientation and width. On the other hand, the east model of Line B (Figure 3.16) is quite different from both the east model of Line A and the west model of Line B (Figure 3.14 and Figure 3.15). This model lies deeper than the others with less magnetic susceptibility and tends to represent a cube shape rather than a tabular shape by its circular feature (Figure 3.11).

The profile of Line C is laid out over a dislocation anomalous feature mentioned earlier (Figure 3.11), therefore, only the southern one is examined. It can be observed that the center of the mode is located over the highest gradient of the profile (Figure 3.17). This model is made from the south toward the north of an anomalous zone, and only modelling of a major anomaly is made. It is clear that the main magnetic body dips toward the north similar to the others mentioned earlier, even modelling in a north-south direction. The

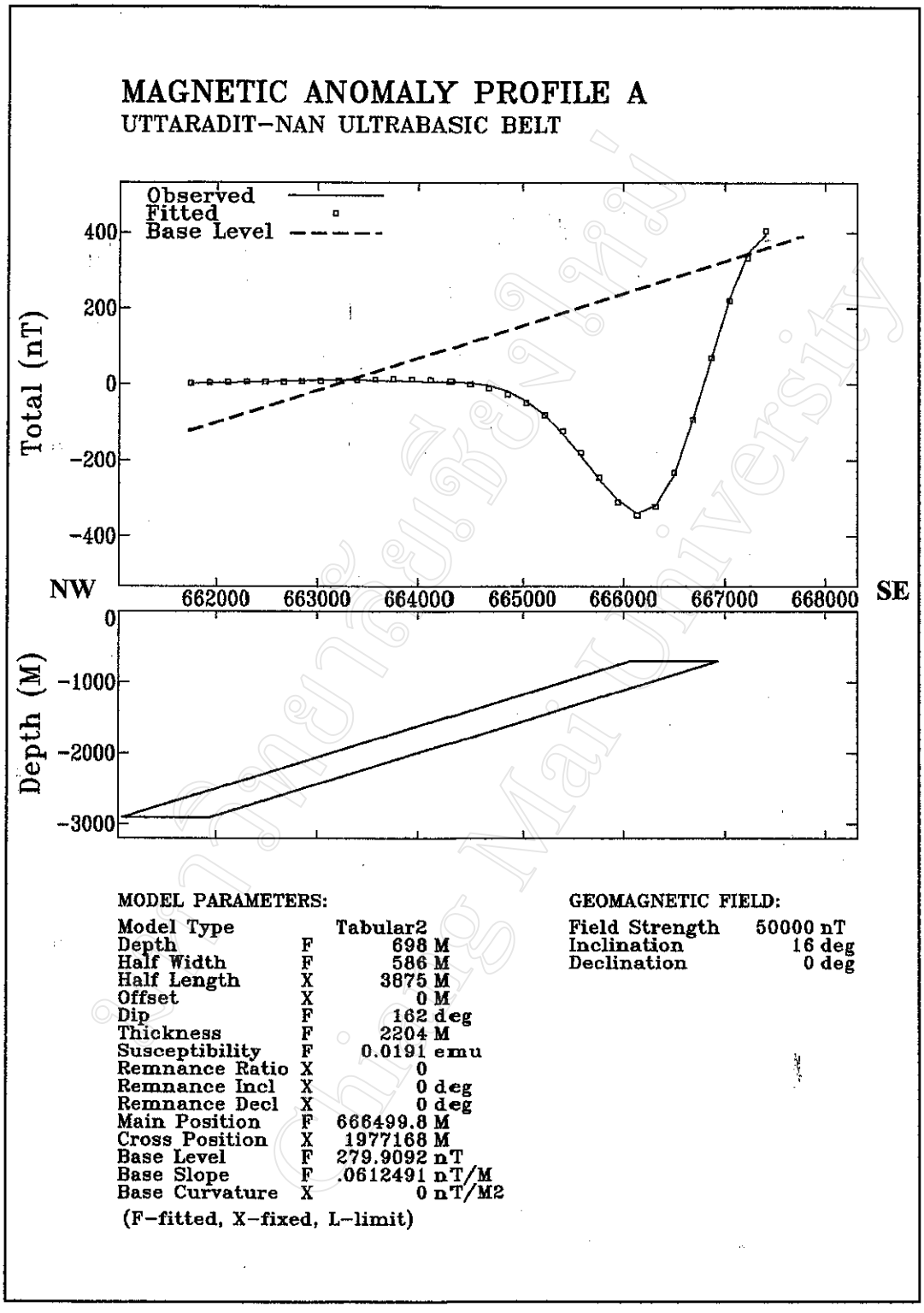

Figure 3.13 Aeromagnetic modelling for Line A.

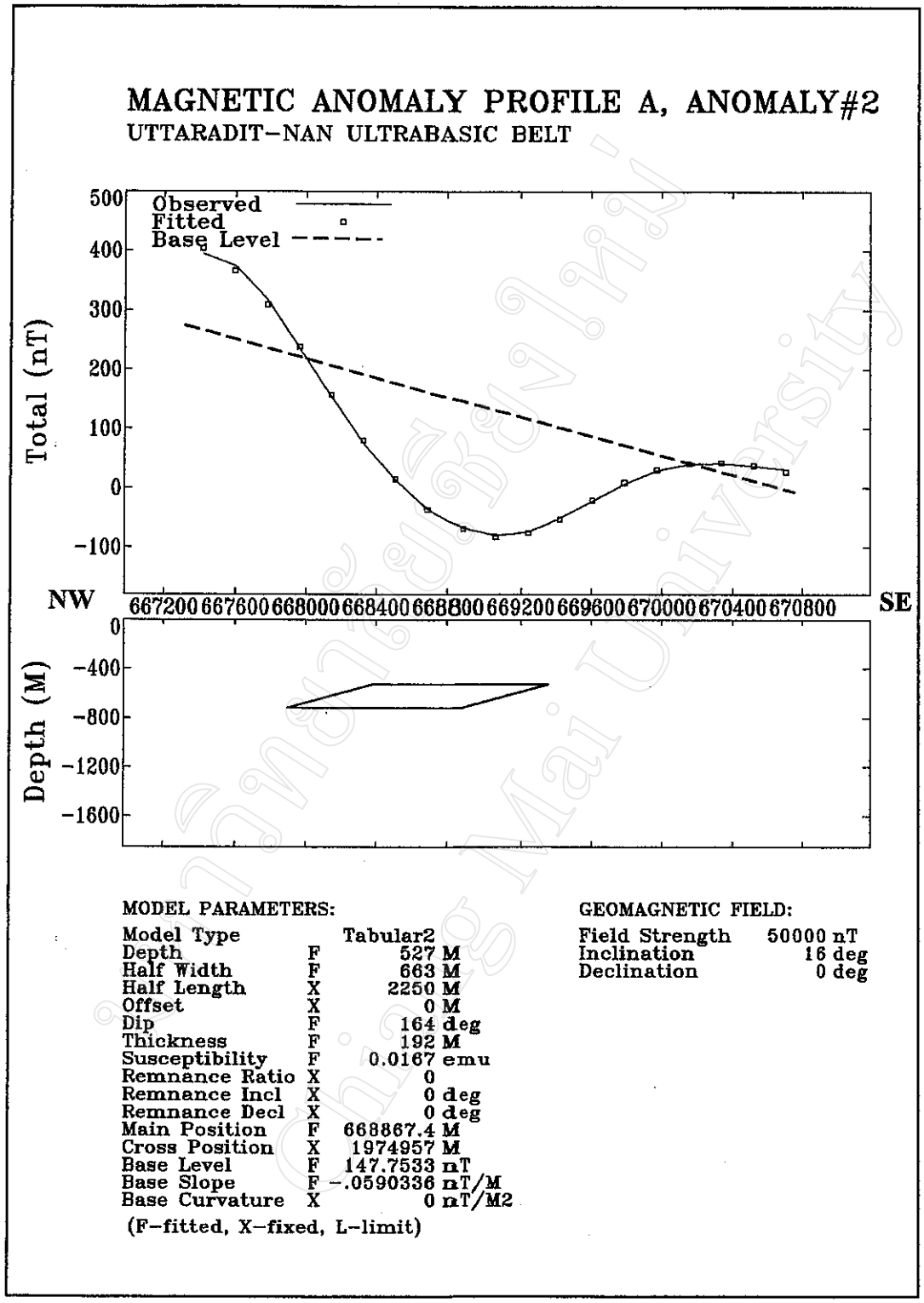

Figure 3.14 Aeromagnetic modelling for Line A part II.

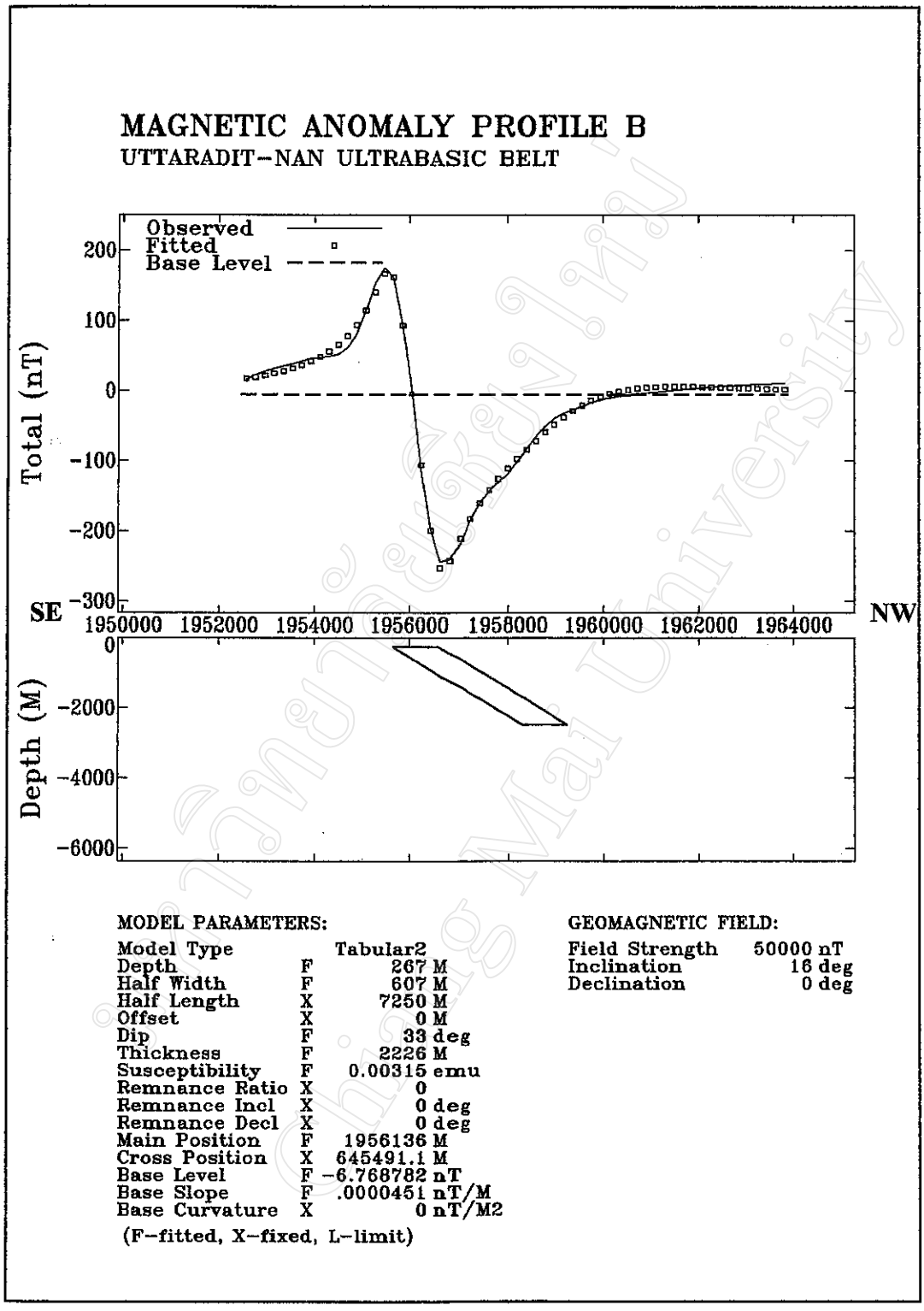

Figure 3.15 Aeromagnetic modelling for Line B.

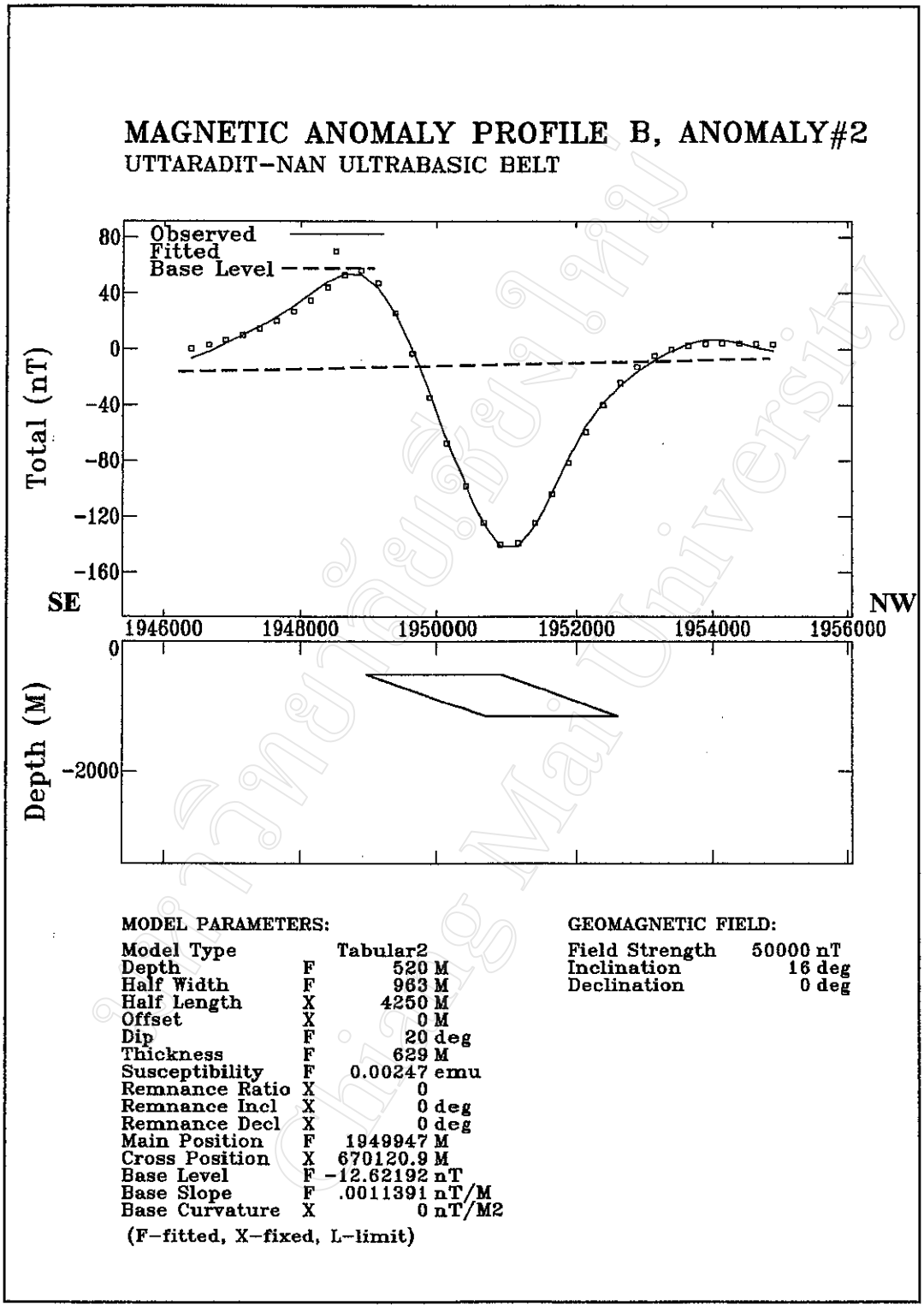

Figure 3.16 Aeromagnetic modelling for Line B part II.

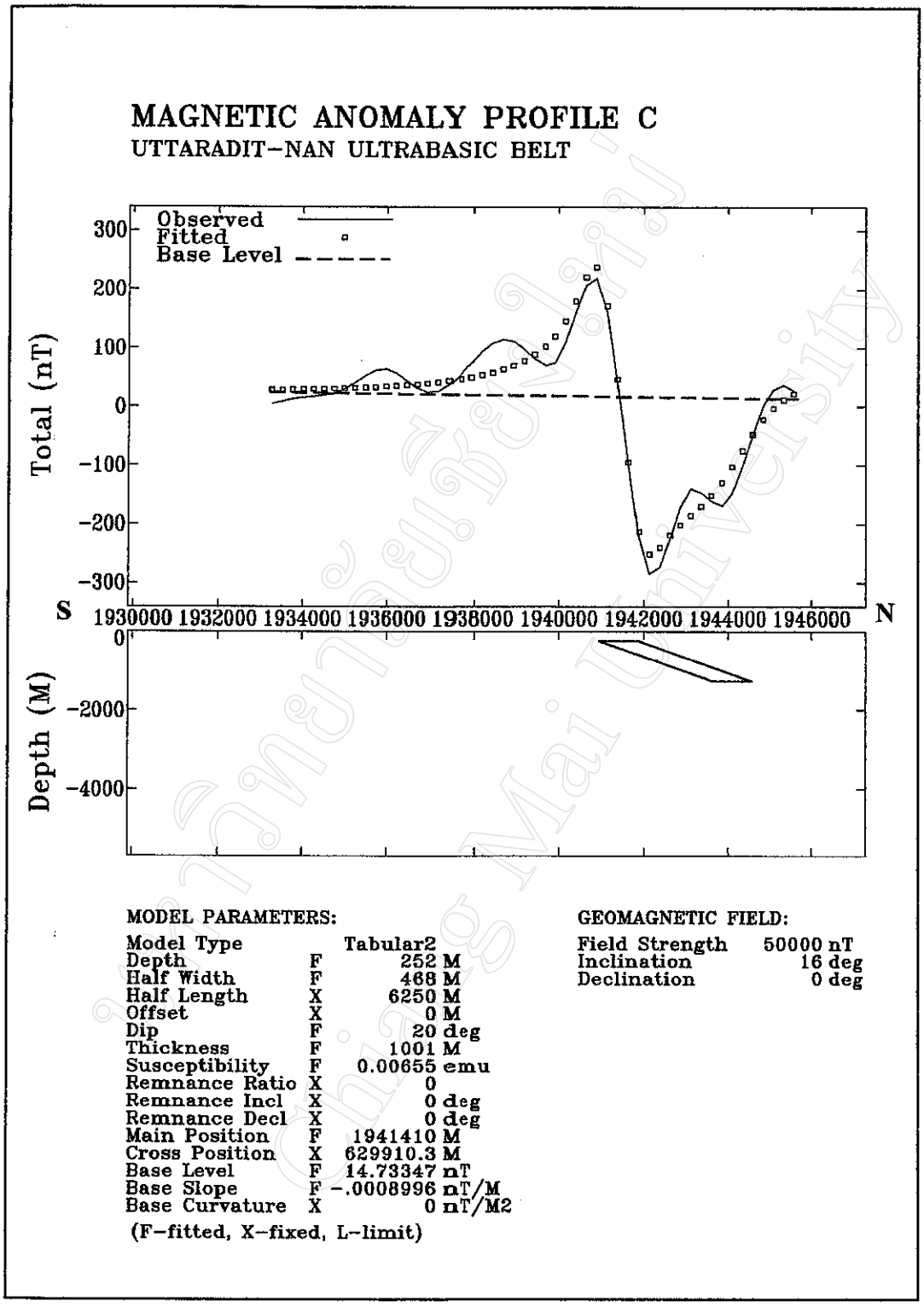

Figure 3.17 Aeromagnetic modelling for Line C.

other magnetic model is located just north of this one and a simple modelling technique (Figure 3.4 and Figure 3.11) cannot separate its anomalies.

Two anomalies with similar magnetic intensities are observed in Line D (Figure 3.11). They are very close to each other similar to those in Line A and Line C but with less intensity and can be separated by this simple modelling technique. In the west, the magnetic body is dipping toward the northwest, 23 degree anticlockwise or 157 degree clockwise (Figure 3.18). A superimposed anomaly is observed on the east of Line D but its intensity is less compared to an interesting one which modelling result shows in Figure 3.19. This magnetic model lies not too deep compared to the west one and extends shallower indicating that it is smaller. The dip angle is also less when considering anti-clockwise where its magnetic susceptibility is almost two times higher.

The northern anomaly of Line E is considered, even though it is not in the study area, in order to compare with the interesting southern one (Figure 3.20). This modelling profile starts from the south toward the north, so only the major anomaly with 90 nT is considered. It shows that this magnetic body is lying at the deepest level compared to all models mentioned earlier. Its great length and thickness cannot be used to indicate its shape as a tabular but an intrusive body can be expected from its circular feature. On contrary, the magnetic body in the south of this line is clearly indicated as an intrusive body (Figure 3.21) by its width and thickness. It lies not as deep as the northern one with far less magnetic susceptibility.

3.1.2 Interpretation techniques for airborne radiometric data

Airborne radiometric survey uses a gamma-ray detector that consists of one or more crystals that scintillate when struck by a gamma ray. The intensity of the scintillation is directly proportional to the energy of the gamma ray, which is a measurable function of the uranium, thorium, or potassium source. By photomultiplier tube, the scintillation is converted to a voltage, and the pulse height is compared with that of a reference source. Results are obtained in reference to diagnostic spectral "windows," as equivalent values for uranium, thorium, and potassium, as ratios between the elements, and as total count.

The geologic source of gamma ray can be related to the elements detected in the individual windows: uranium possibly from a uranium ore deposit or from a uranium-bearing pegmatite, thorium possibly from a monazite-bearing sand, radiopotassium possibly from a granitic pluton. The choices are many, so are the applications in reconnaissance mapping, and so are the types and sources of radiometric noise. Noise associated with radiometric surveying changes with altitude, but on-board data processing and calibration provide

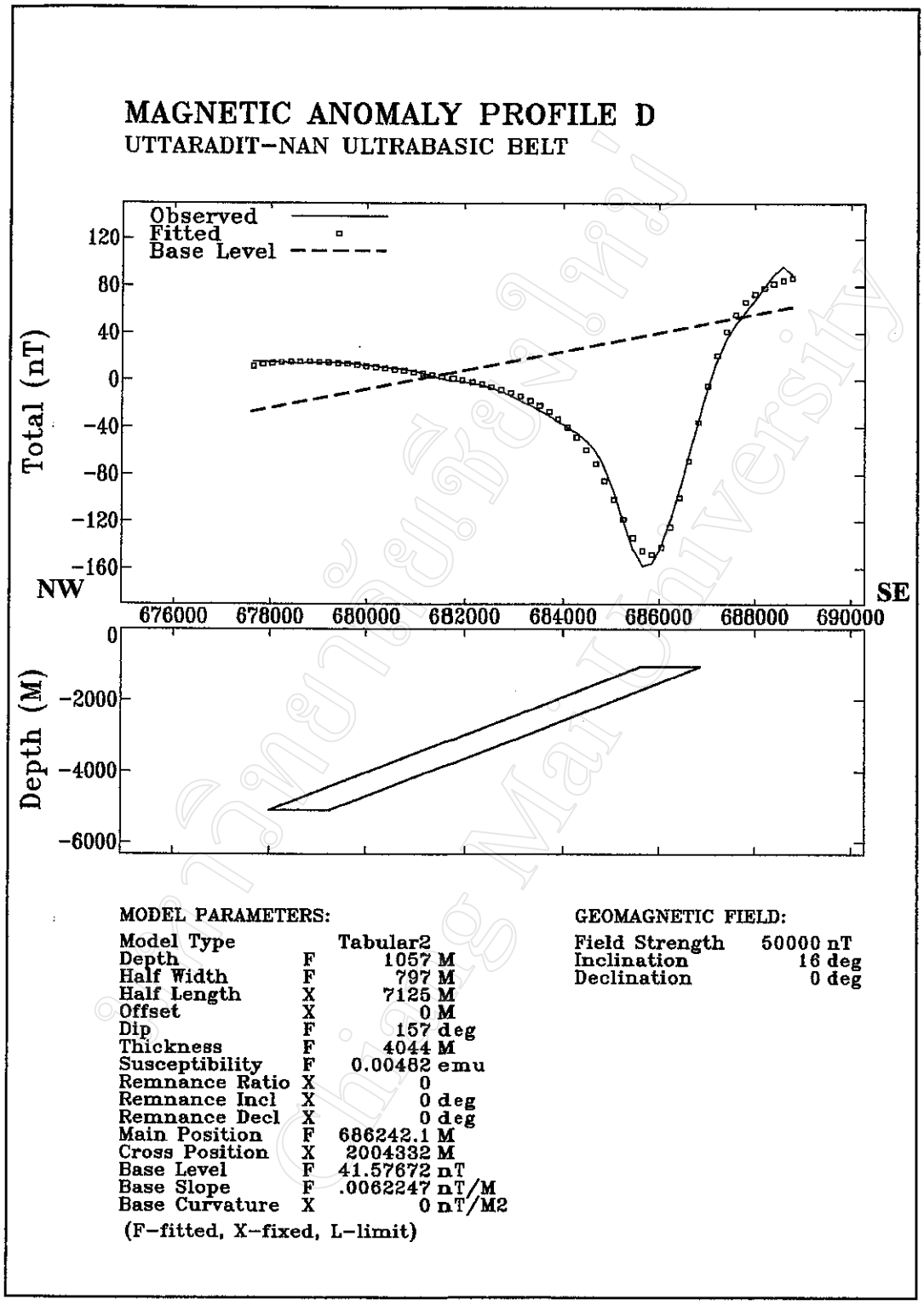

Figure 3.18 Aeromagnetic modelling for Line D.

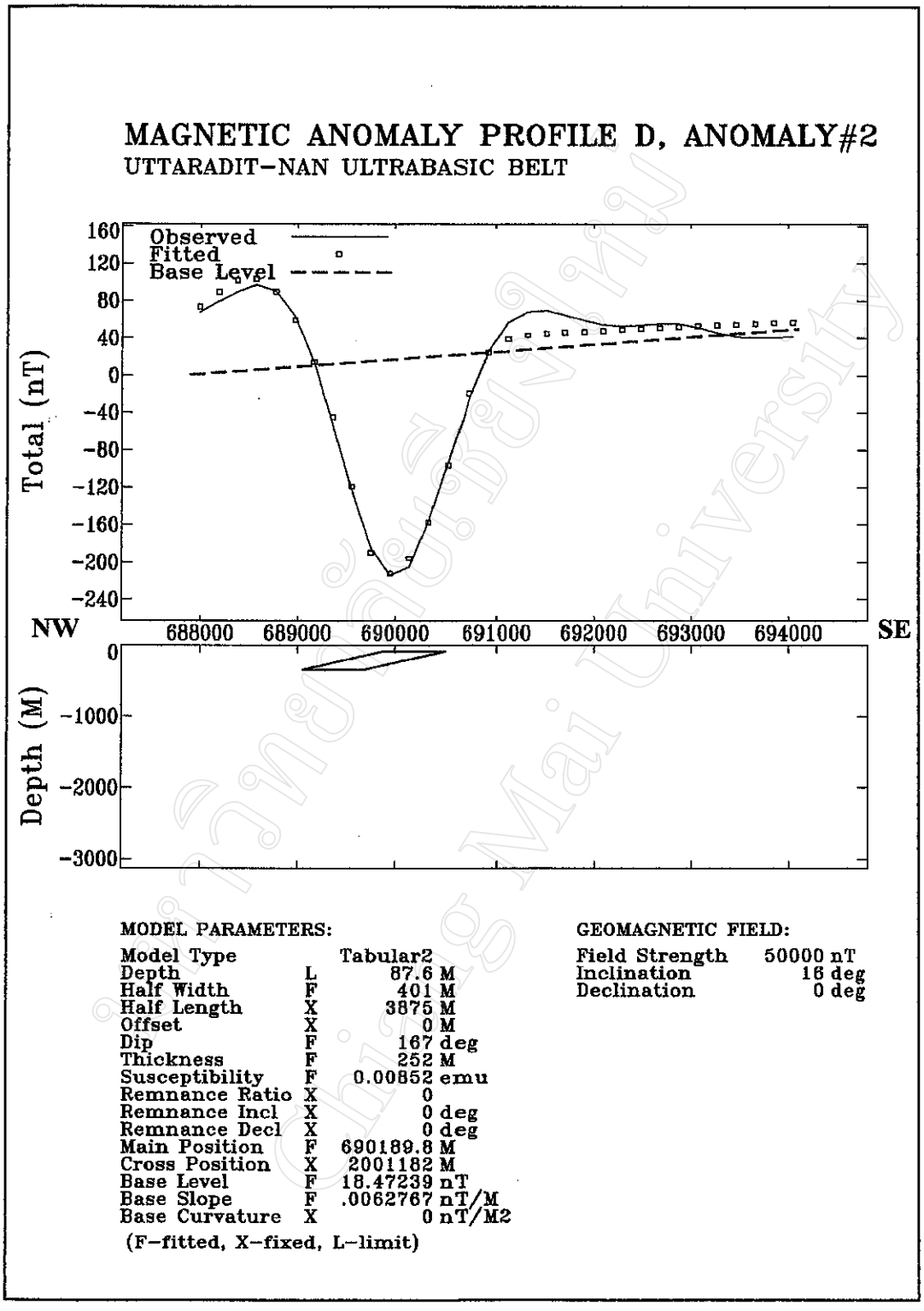

Figure 3.19 Aeromagnetic modelling for Line D part II.

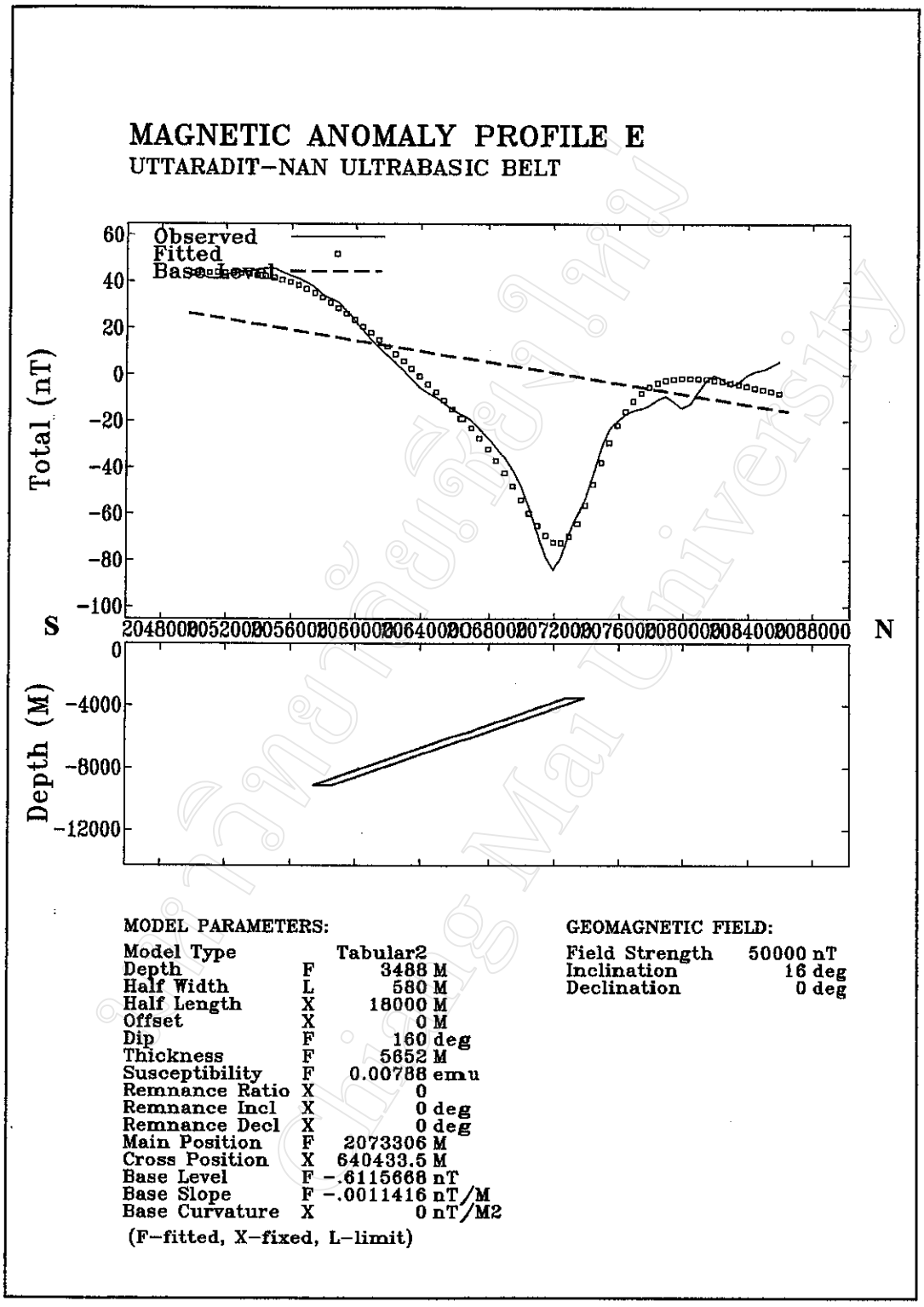

Figure 3.20 Aeromagnetic modelling for Line E.

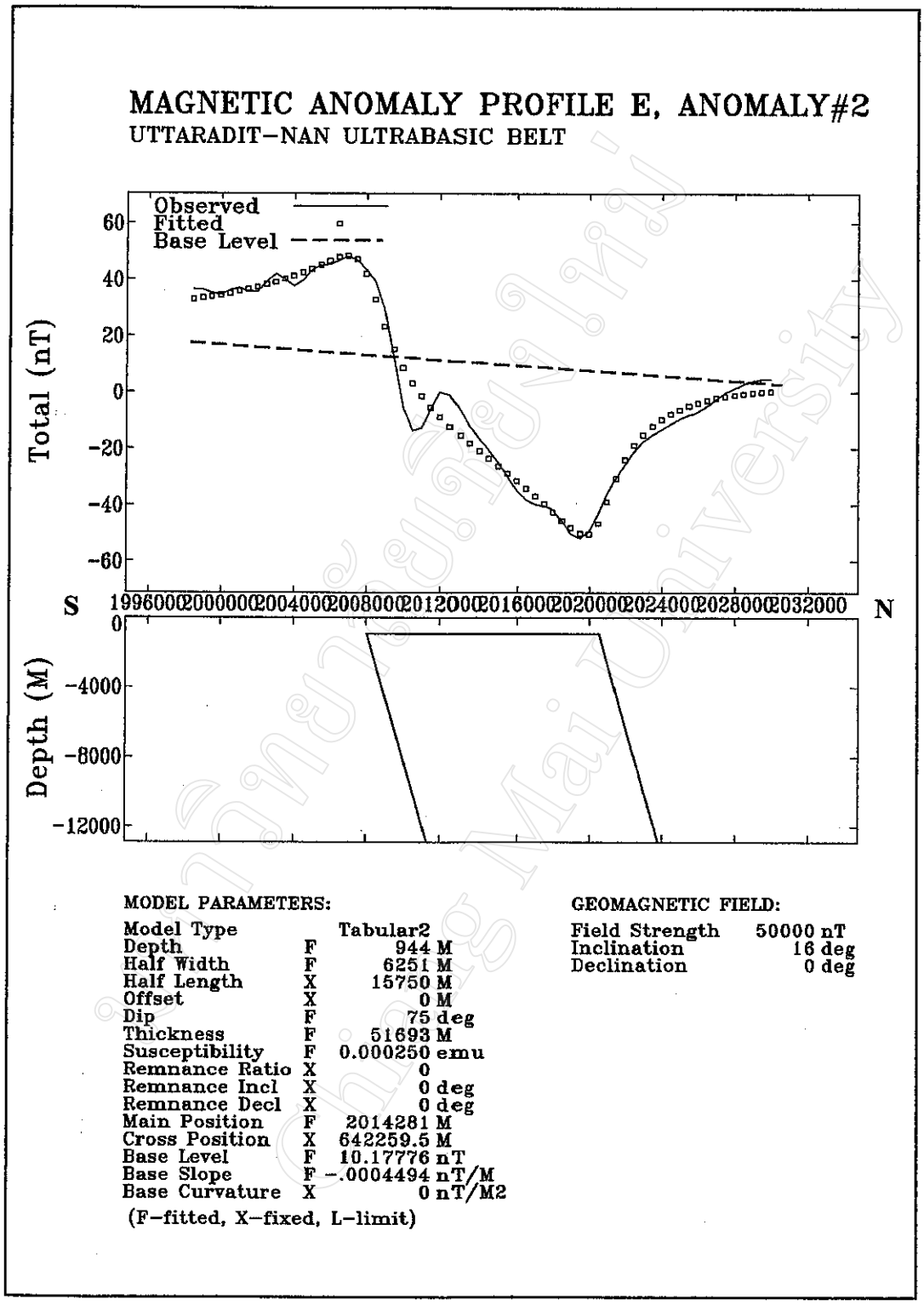

Figure 3.21 Aeromagnetic modelling for Line E part II.

filtering of noise. However, there are some limitations of airborne radiometric survey. Potisat (1980) summarized some of these limitations for both advantage and disadvantage considerations:

1. Thickness of overburden causes dilution of gamma ray intensity. Detection of gamma ray over thick soil, over 50 cm, may be impossible. Accordingly, investigation on alluvium or desert and particularly in wet tropical area is almost useless.

2. Moisture in soil and weather may obscure gamma-ray intensity as well. Radiometric anomalies on a rainy day may be 50% less than on sunny day, for example, and intensity will increase to 75% on the second day, and 90% on the third day after raining, respectively. Gamma-ray intensity measured over dry soil may be 3-4 times greater than that of wet soil because rain erodes radon daughters down from hemisphere. For moist soil, 13-37% increase in moisture causes a total count decrease of 15%, and intensity, measured from Bi^{214}, decrease of 50%.

3. Dense forest along the equator can also reduce penetration ability of gamma ray. Height of trees may cause errors in height corrections, and forest biomass is a reducer, absorbing gamma ray very well.

4. Intensive weathering in tropical area causes some problems in interpretation, because radioelements such as uranium and thorium will be washed-out from the surface, even though the underlying rock contains uranium or thorium. In case of lateritic soil or laterite or bauxite, interpreter may face with abnormal anomalies, normally of thorium more often than uranium. However, field check would indicate that most of them are false anomalies, except for uraniferous laterite.

5. Undulating topography limits ability of fixed-wing airplane but helicopter can be used instead. However, the cost is really expensive. Moreover, inability to keep the mean terrain clearance of plane elevation may cause false anomalies. Therefore, interpreter must be careful on anomalies detected above mountainous regions. In order to decrease these limitations, altimeter may be applied, together with background value measurement and instrument calibration.

The radiometric signal is greatly affected by soil and other kinds of overburden. Gamma radiation is completely absorbed by about 50 cm of soil and rock. Areas of transported soil and alluvium are therefore likely to mask the underlying gamma radiation. Residual soil, on the other hand, may still contain enough original radioactive rock component to provide a signal. The problem arising from irregular "cover" is easy to visualize. Bare rock ridges and soil-covered hills will show a higher gamma radiation than stream courses

and alluvial plains, unless the alluvium happens to contain transported radioactive minerals. Vegetation and paddy field are influencing factors as well. They are geophysical "overburden" because they absorb radiation to some extent (Killean, 1979).

Data from gamma-ray spectrometer surveys are plotted as coloured contour maps. Contours are commonly based on the total count rate and on the count rate for each channel (Figure 3.22). The areas shown in Figure 3.22 is the same as that shown in Figure 3.6 and Figure 3.7 for aeromagnetic survey.

Interpretation of airborne radiometric data is best done with as much prior knowledge of the overburden conditions, rock types, and terrain as can be obtained. However, on the basis of a reconnaissance map, a radiometric anomaly may be explained entirely by the position of a granite knob surrounded by alluvium or by a high hilltop, or it may have a spatial connection with known or suspected pegmatite dikes (Peters, 1987). In general, gamma radiation from arkosic sandstone, for example, should show a potassium anomaly as well as uranium anomaly, whereas gamma radiation from a phosphatic-chert with small uranium content would not normally show the radio-potassium components. Pegmatite dike or leuco-granite of high potassium feldspar mineral is strongly shown by high potassium. Granite may be interpreted from either high uranium or thorium but the weathered granite has more potassium content (Surinkum and Paiyarom, 2000). Non-anomalous zone may be observed over the ultramafic terrain for all radioactive elements because their atomic sizes cannot be incorporated in rocks formed at the deeper level. Two different interpretations are made in this study: intensity contrast and correlated intensity.

3.1.2.1 Intensity contrast

Shaded contour maps of radiometric data were used to identify and delineate radiometric anomalies reflected from the rock types, topography and drainage patterns. Normally, one or more elements, U-Th-K, reaching half of the total range, is considered simultaneously first. Comparing to the similar formation locally will then outline each individual element expression.

The intensity contrasts of all airborne radiometric elements of the study area show that low radiometric intensity, for example less than 1Ur, is located over the U unit, the reservoir, and the J unit and Qa (Figure 3.22a and Figure 1.4). Two different high radiometric areas, for example more than 3 Ur, are found as elongated zones in the northwestern part, while circular zones are found in the southern part of the study area. Uranium data, on the other hand, does not correspond with the total count (Figure 3.22b). Uranium anomalous zones are more widespread and have different shapes both for high, more than

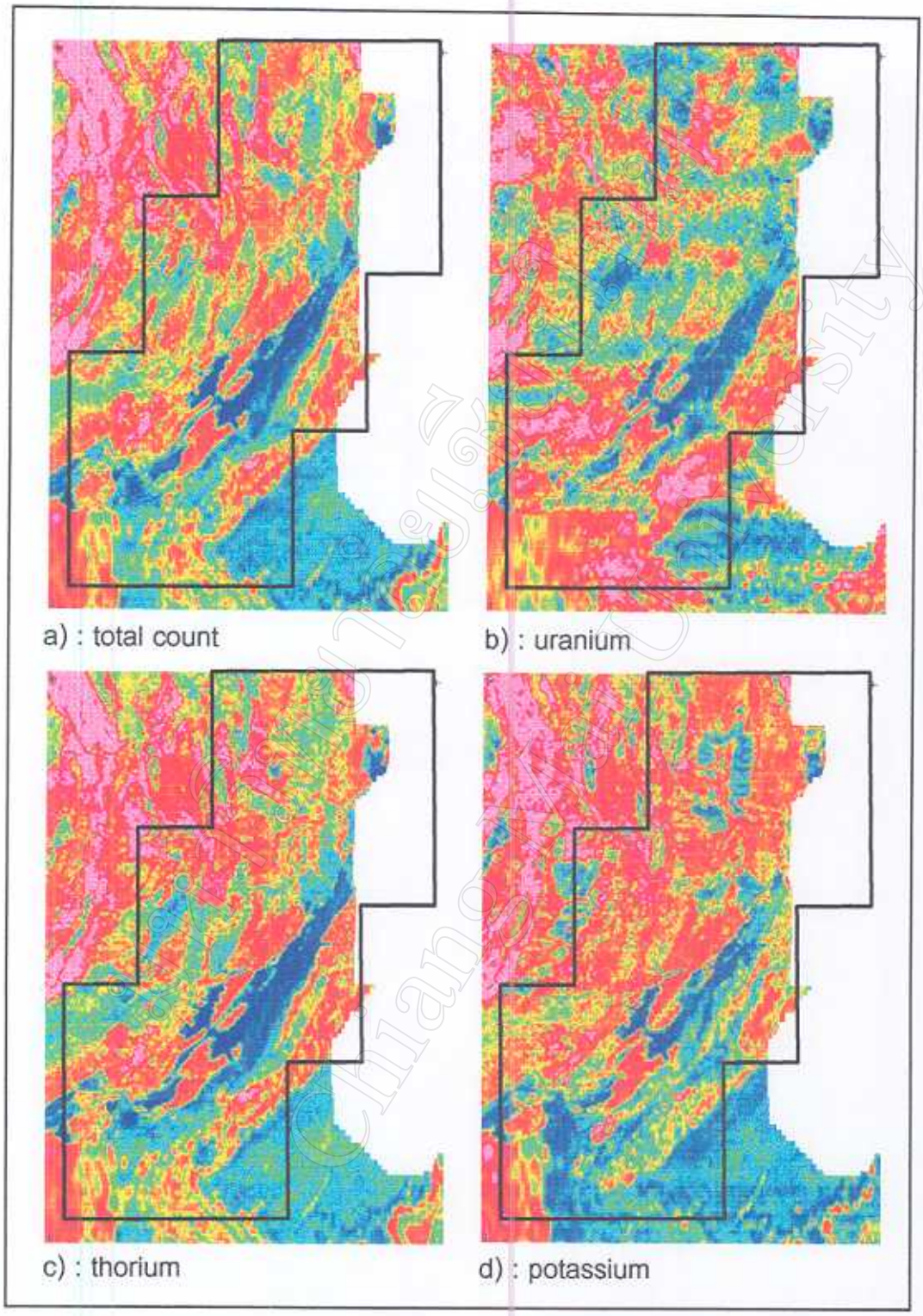

Figure 3.22 Airborne radiometric data of the study area.
(scale referred to Figure 2.4 - 2.7)

1.75ppm, and low uranium contents (less than 1ppm). An elongated zone in the northern part reflected from total count cannot be recognized easily from uranium anomaly but the circular zones in the south are clearly outlined. Thorium data reflects the same pattern as it does on total count (Figure 3.22c), especially on the high thorium parts (more than 11ppm). In contrary, low radiometric expression of thorium is more widespread than that of total count. These phenomena are not found for the potassium content (Figure 3.22d). Both high (more than 11%) and low (less than 3%) potassium zones are more confined and clearly outlined over mapped units such as the U unit but not over the Qa unit.

3.1.2.2 Cooking technique

This technique is used in this study in order to examine the intensity of related radioactive elements. The red colour is assigned to uranium, where green and blue are to thorium and potassium respectively. Their relationships are examined where light colour reflects high intensity of both elements and dark colour reflects the low intensity. Pairing of U, Th and K are examined to see how they relate to each other and how they are different from the total count (Figure 3.23a). The relationship between U and Th shows that both are concentrated in similar areas to the total count (Figure 3.23b). Two different anomalous zones can be observed: an elongated zone and circular zone. They were assigned for comparison as E-1 to E-4 for elongated zones and C-1 to C-4 for circular zones. There is also a distinct V-shaped feature south of E-1 (Figure 3.23b) indicating low uranium and thorium as it is found over the U-unit. However, this feature is not clearly identified by the Th+K (Figure 3.23c) and K+U (Figure 3.23d) pairs. However, the C-4 is clearly defined by both pairs that may indicate more potassium alteration over this C-4.

Where U+Th and Th+K are concentrated on the circular feature, K+U reflects two more features, C-5 and C-6 (Figure 3.23d). These relationships show that high K+U are located over those features, indicating some potassic alteration product. It can be interpreted as intrusions at depth where definite expression should be outlined by other means.

All positive and negative anomalies of the radiometric data are correlated to mapped units and also expressions resulting from subsurface geology. In the northern part, low radiometric areas are reflected from the U unit, Qt and Qa (Figure 3.24). High radiometric areas are found in the northeast corner and along the western part of this area. The northeast one cannot be related to surface geological information but the high of potassium element can be interpreted as some intrusions. This can also be interpreted for a circular anomaly located within the areas of the Mzv and the Jpk in the west. Other

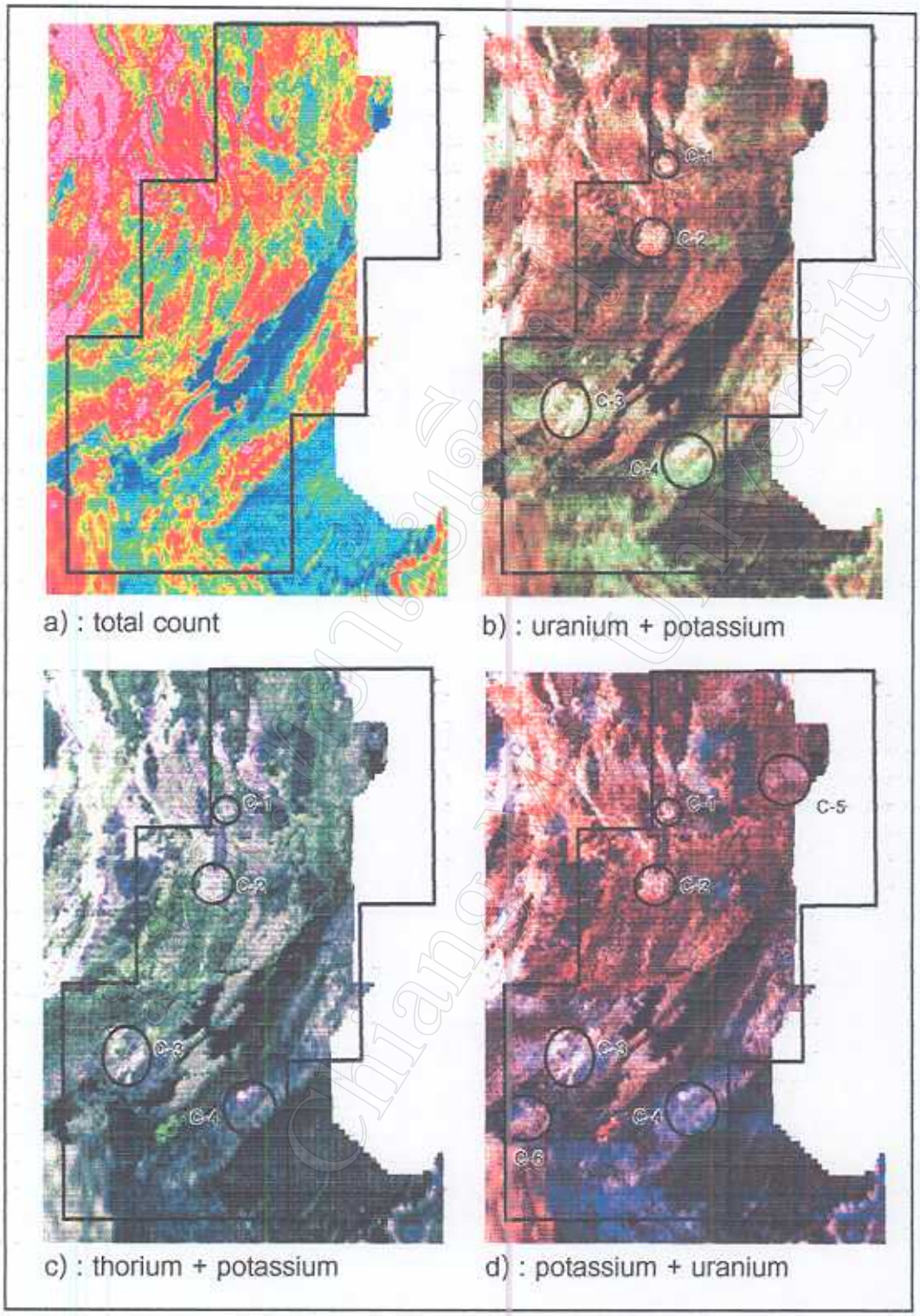

Figure 3.23 Airborne radiometric data enhanced by cooking technique

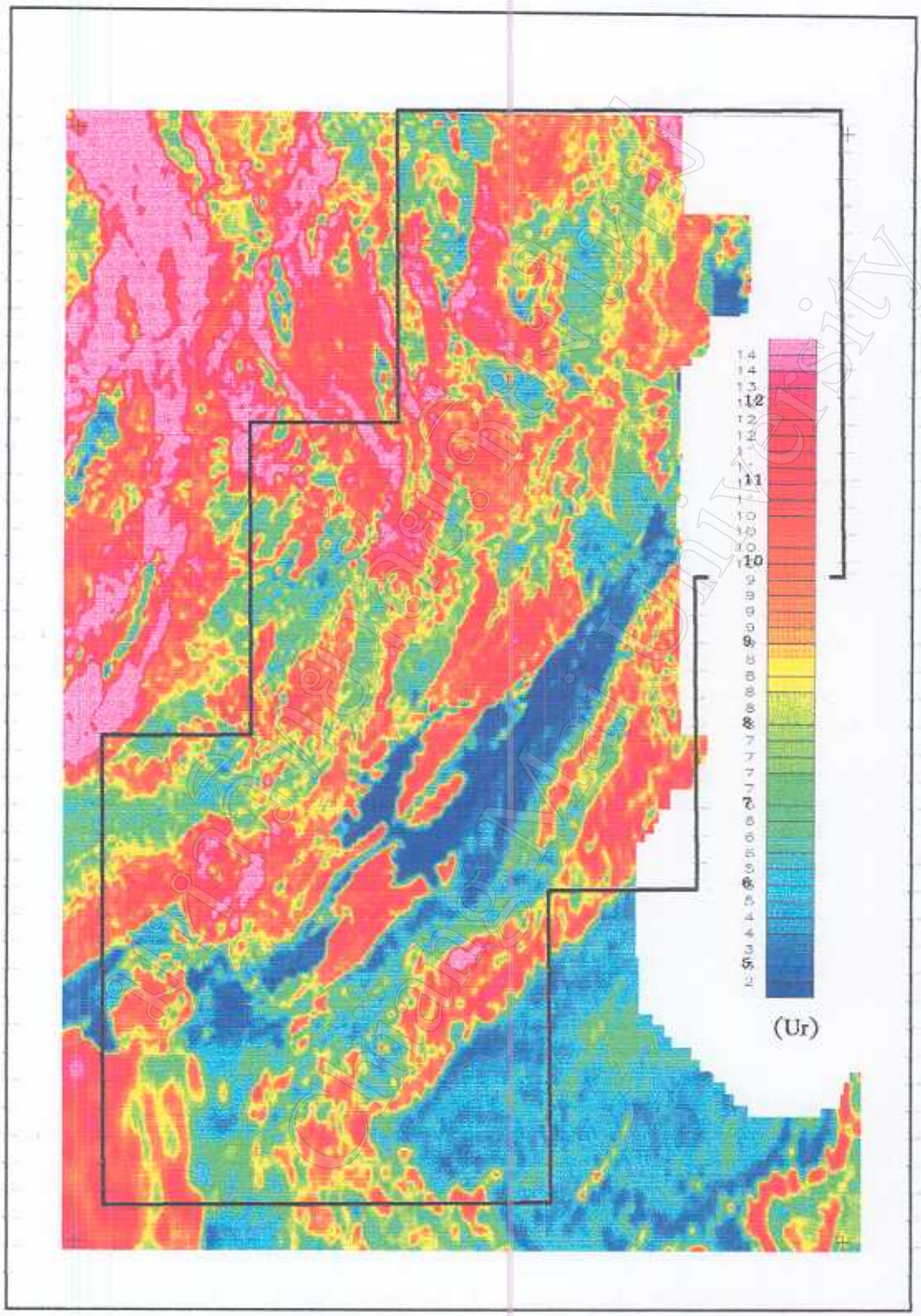

Figure 3.23a Airborne radiometric data enhanced by cooking technique.
(total count)

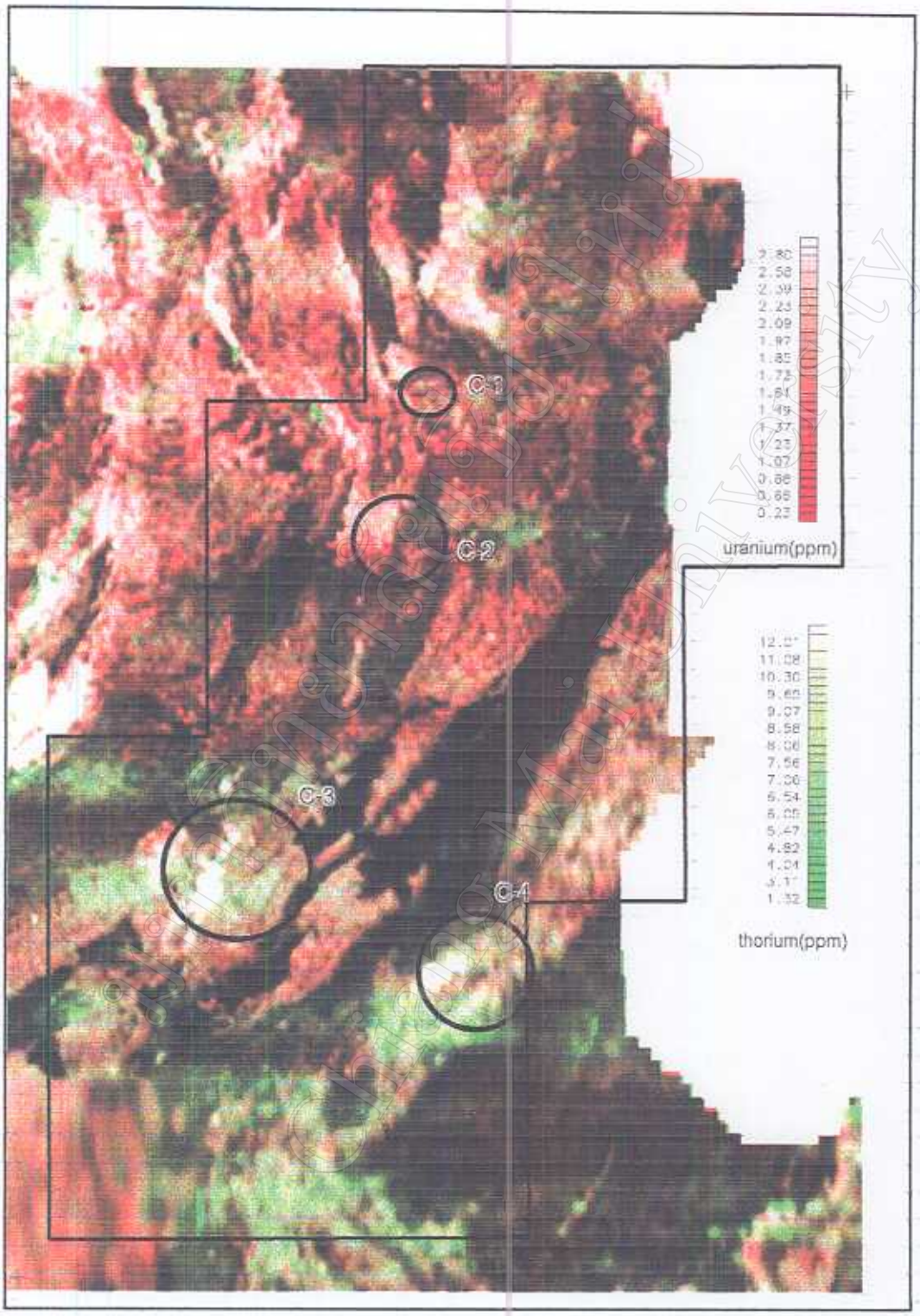

Figure 3.23b Airborne radiometric data enhanced by cooking technique.
(uranium and thorium)

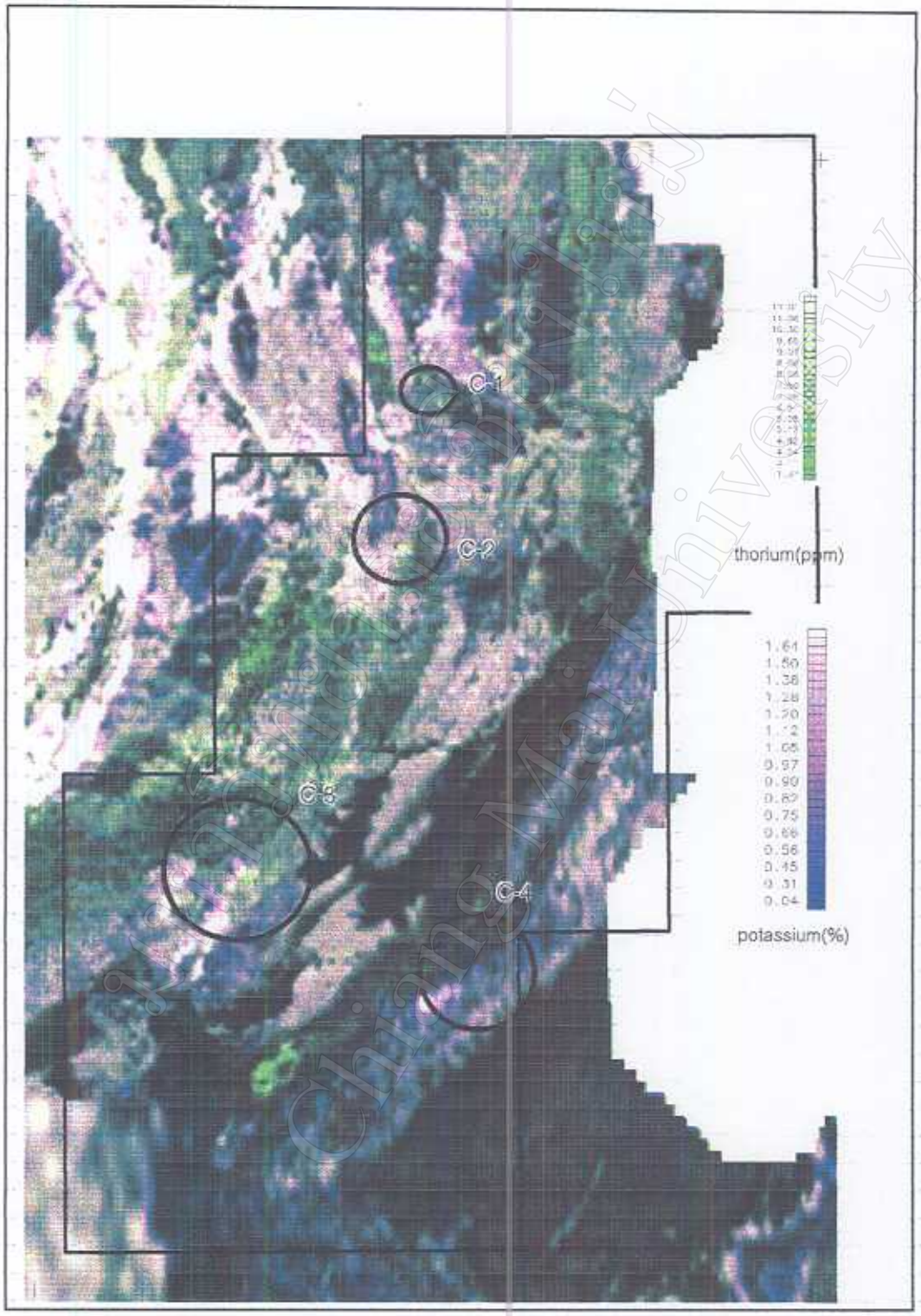

Figure 3.23c Airborne radiometric data enhanced by cooking technique.
(thorium and potassium)

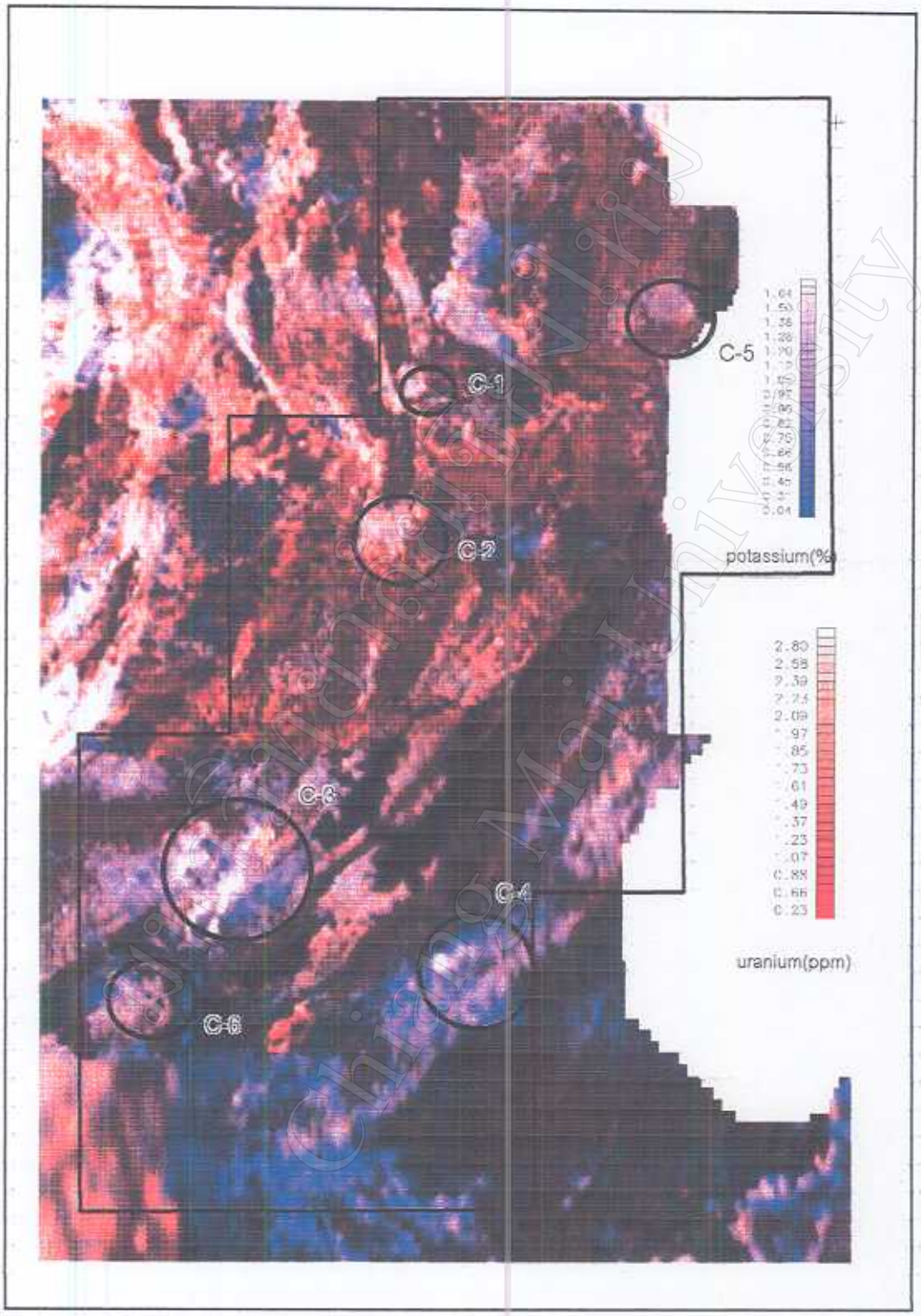

Figure 3.23d Airborne radiometric data enhanced by cooking technique.
(potassium and uranium)

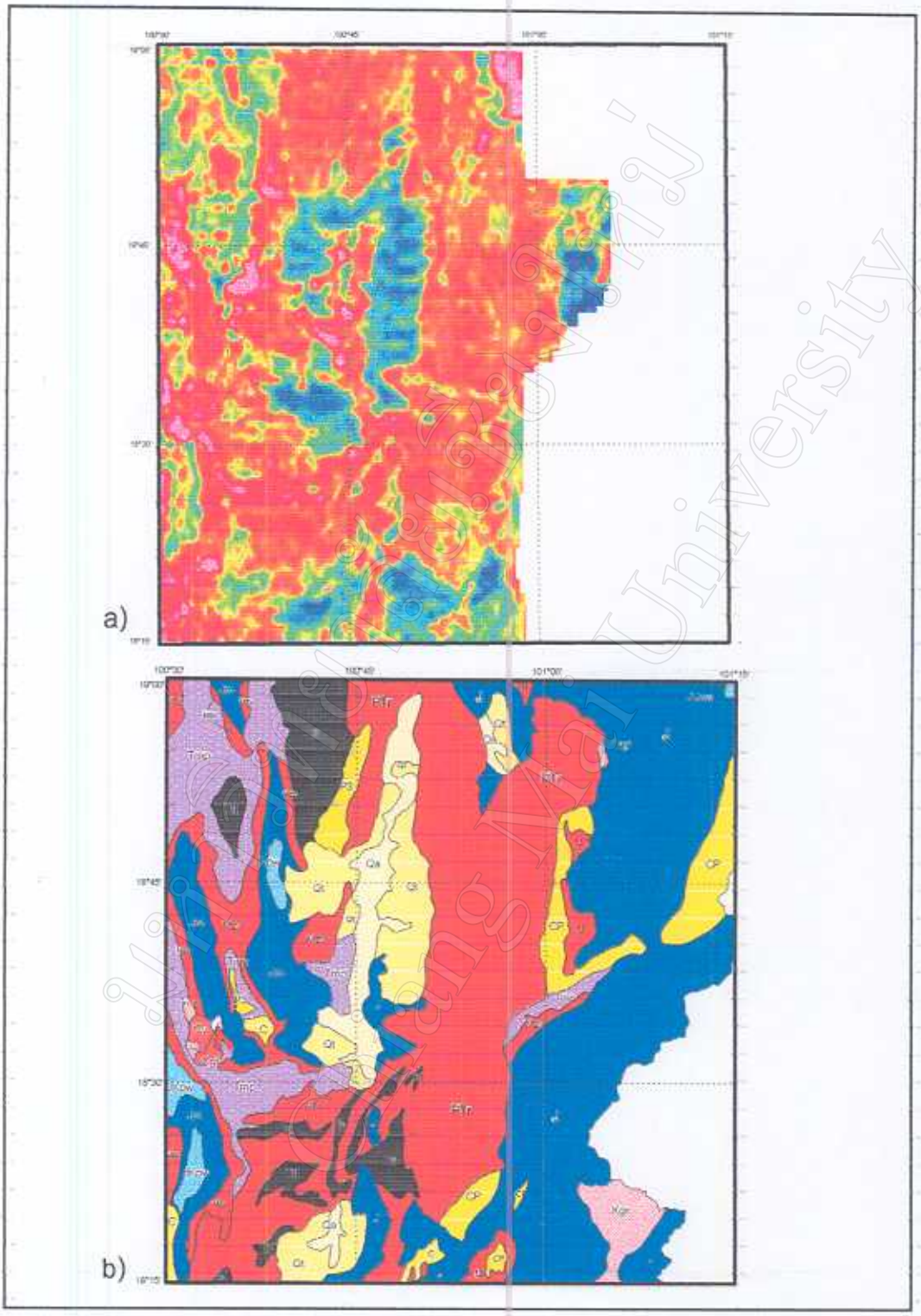

Figure 3.24 Correlation of radiometric (potassium) anomalous areas (a) and geology of the northern part (b).

(symbols are the same as those in Figure 1.5 and scale referred to Figure 2.5)

elongated features are found over the Jpk in the west indicating high radiometric content within this unit.

Total count radiometric data of the central part shows that NE-SW trending is the major geological structure of this area (Figure 3.25a). A younger basin, identified by low radiometric (less than 1Ur), is located in the western most part and, to the east, volcanic areas with high radiometric elements (more than 3Ur). In the middle part, radiometric data represent sedimentary sequence of the C and SD units. They also indicate that the ultramafic rocks of the U-unit are more widespread. There should be at least other two elongated zones parallel to the one north of the reservoir marked by W symbol. Other major unit of ultramafic rock should be located north and west of the north one where the PTr and C units are outlined in the geological map shown in Figure 3.25b.

There are many radiometric signatures different from the mapped units in the southern part (Figure 3.26). The most interesting one, a circular feature, is located in the east of this area where its radiometric products, especially K, extends toward a NE direction. There is no surface evidence indicating any intrusion or a significant alteration except some lateritic soil. This potassium anomaly is coincident with high peak magnetic anomaly shown in Figure 3.10, where polymetallic mineralization normally occurs. The Mzv units outlined in the geological map also reflect different radiometric characteristics. Mzv-1 is correlated with rhyolite where illite is mined (Surinkum and others, 1995). The anomalous zones nearby are correlated with granite (Tgr) and the outlines of Tgr should be reconsidered according to the radiometric expression in this area. This expression is also found over the Mzv-3 but not the Mzv-2 and Mzv-4.

3.1.3 Interpretation technique for helicopter-borne electromagnetic data

The airborne electromagnetic data are not fully accomplished over the entire study area because it was done over a specific high potential area as mentioned earlier. The procedure of this survey is also set for mineralization associated with conductors. Two different types of anomalies are being considered. There are conductive degree or amplitude classification and magnetic associated conductor.

3.1.3.1 Amplitude classification

Normally, amplitude of both inphase and quadrature components in electromagnetic survey is used to classify type of conductor, a higher signal a better conductor because these components are reflected directly from the conductance of the conductors. In this study, three different classes are examined, good (16-32mS), moderate (8-16mS) and poor (4-8mS) conductors. Stacked profile shows that each component is plotted according to their survey

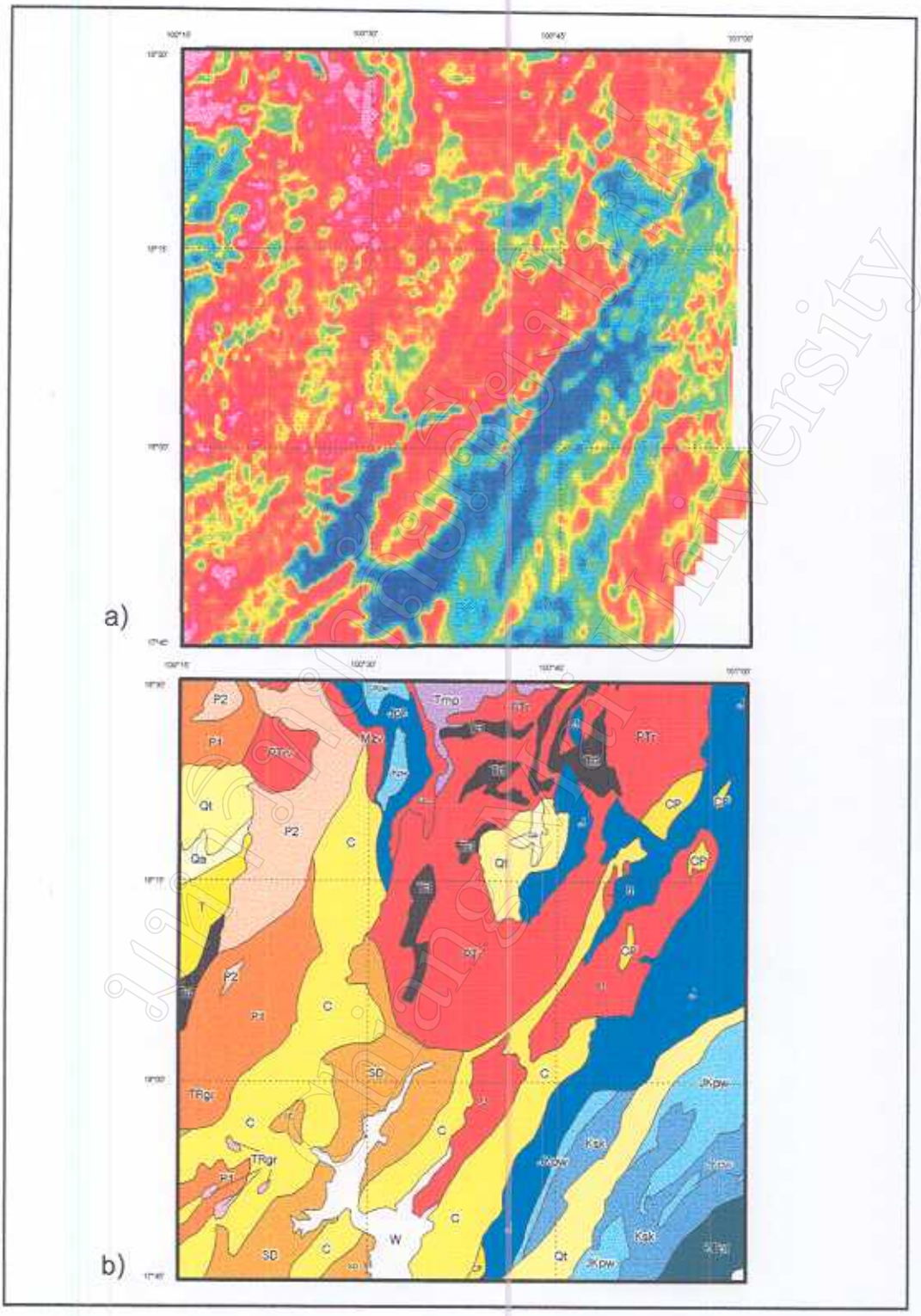

Figure 3.25 Correlation of radiometric (potassium) anomalous areas (a) and geology of the central part (b).

(symbols are the same as those in Figure 1.6 and scale referred to Figure 2.5)

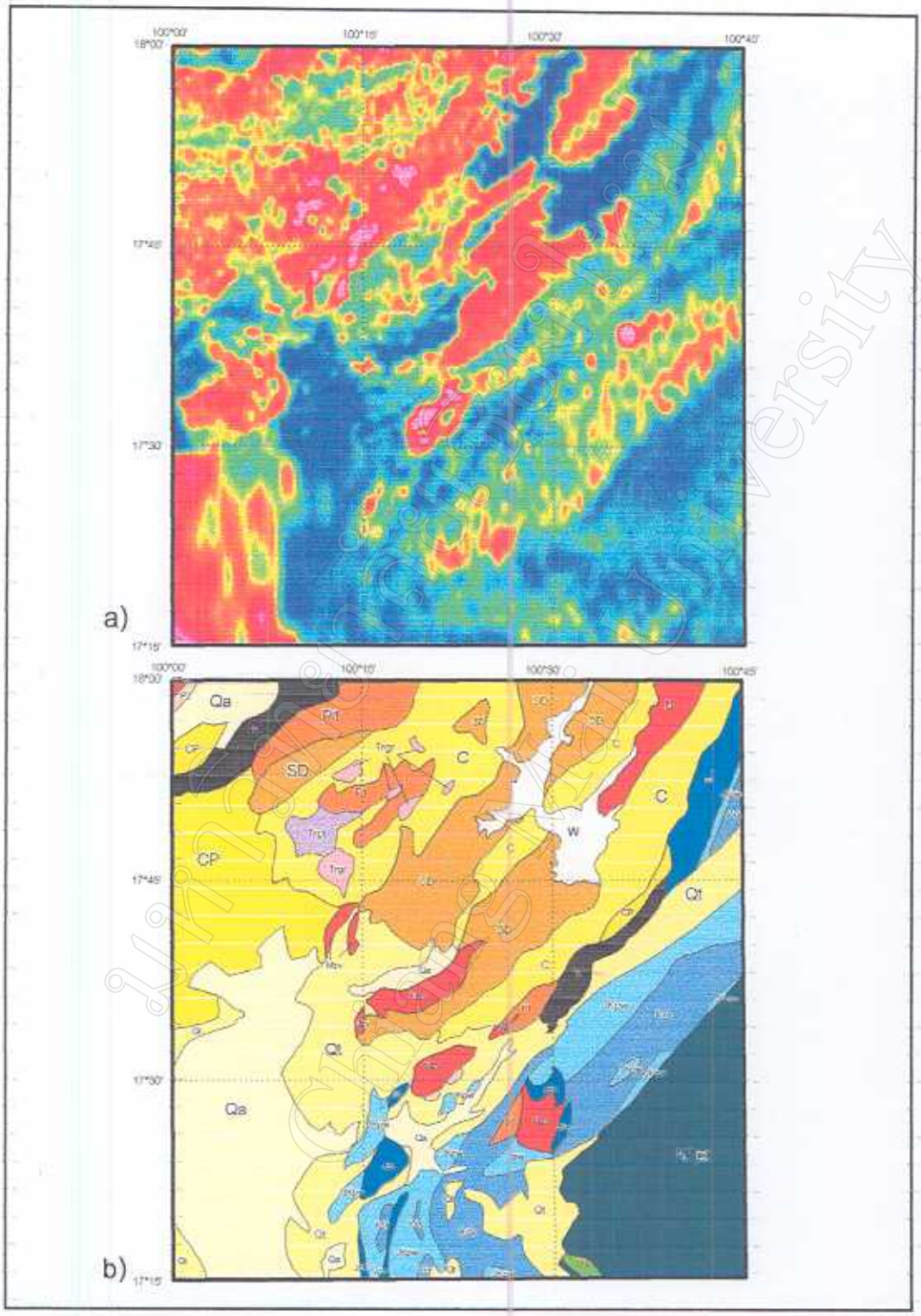

Figure 3.26 Correlation of radiometric (potassium) anomalous areas (a) and geology of the southern part (b).

(symbols are the same as those in Figure 1.7 and scale referred to Figure 2.5)

lines and vertical scale is set for their amplitude (Figure 3.27). The amplitude is scaled as ppm or part per million of the transmitting signal, and trough-like shape represents an anomaly (Beck, 1981). In this area, the good conductor is located in the southernmost survey line where both inphase and quadrature components are high in amplitude. Toward the north, less amplitude indicates moderate conductor and poor conductor, respectively.

3.1.3.2 Magnetic associated anomaly

The magnetic associated anomaly is reflected from a conductor that has high magnetic susceptibility (Palacky and Stephens, 1990). Degree of magnetic susceptibility is characterized by the reverse degree of an inphase component; the higher the reverse, the higher the magnetic susceptibility. Plotting both components on a stacked profile where negative on amplitude scale indicates a normal and positive indicates reversal amplitude comparatively identifies this character (Figure 3.28). The magnetic associated conductors are found lying northeast southwest along the west flank of a mountain at the middle of Ban Khung Yang area. Toward the west of this magnetic associated zone, quadrature components are also reversed due to a conductive overburden of Quaternary alluvial or paddy field east of the village of Ban Khung Yang to Ban Klang in the north.

3.1.4 Correlation using integrated data

Integrated radiometric and magnetic data can recognize alternating layers of andesitic and rhyolitic tuffs. The rhyolitic layers exhibit relatively low magnetic intensity but high radiometric characters whereas andesitic layers give strong magnetic response and relatively weak radiometric response.

Magnetic anomalies are elongated in the strike direction of the volcanic sequence. Spotty texture, incoherent, relatively short wavelength characters of magnetic anomalies are shown over volcanic terrain. In felsic to intermediate volcanic terrains, some alteration zones may be related to mineralization. Studying variation of radiometric responses within such terrains is, therefore, useful.

The marked change in potassium content or radiometric ratio could be used to indicate the mineralization processes involving the geochemical alteration. The hydrothermal alteration product of rhyolite is clay deposit such as at the Khao Kiu Mamun area north of Uttaradit (Surinkum and others, 1997). This clay deposit is recognized by local enrichment of potassium that is reflected in the spectrum of Landsat imageries (Leungingkasoot and Techawan, 1997). Thus a regional geological framework of the study area can be outlined from these characters and further ground check can be made on more specific area rather than following a random procedure.

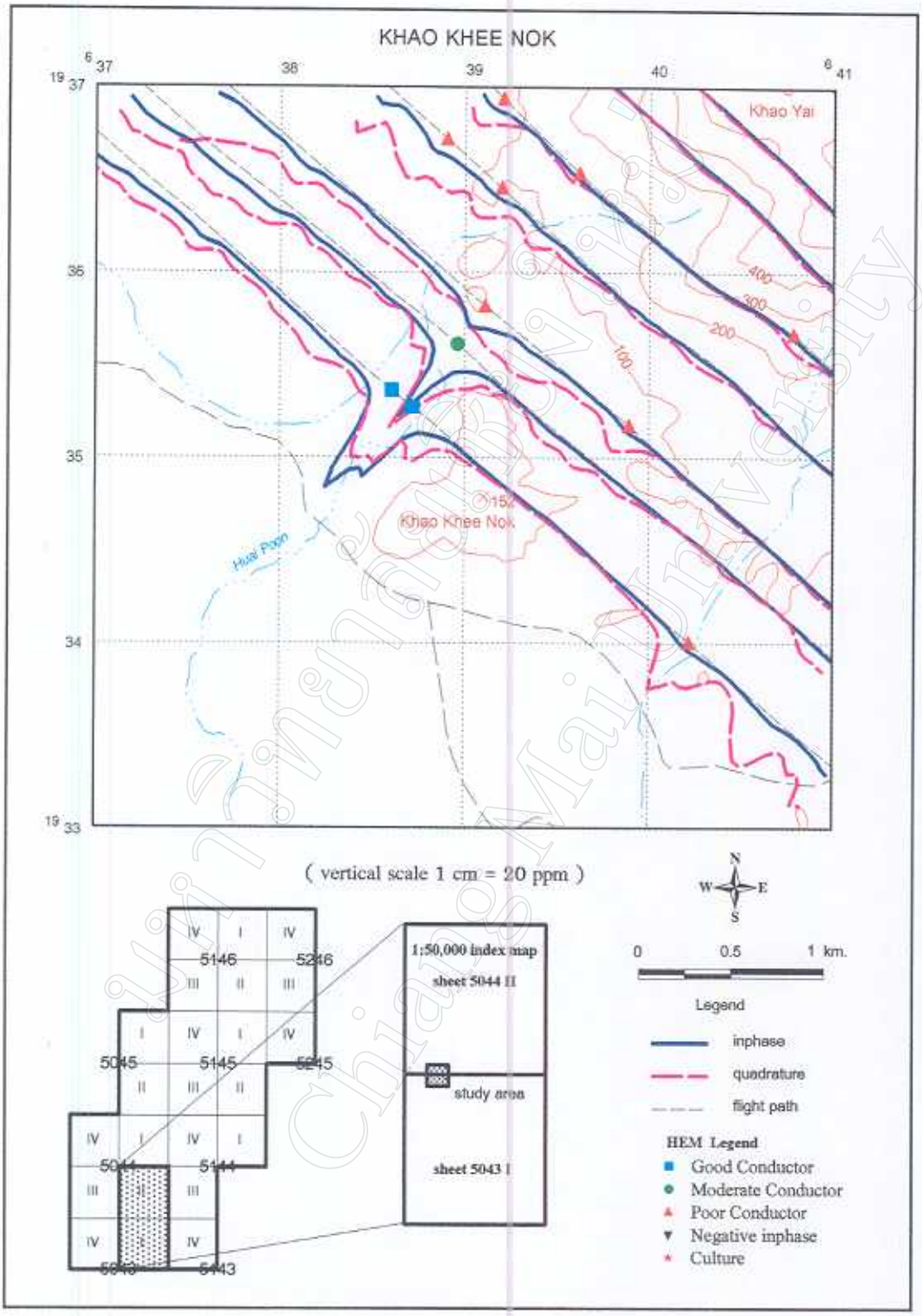

Figure 3.27 Helicopter-borne electromagnetic stacked profile over conductors.

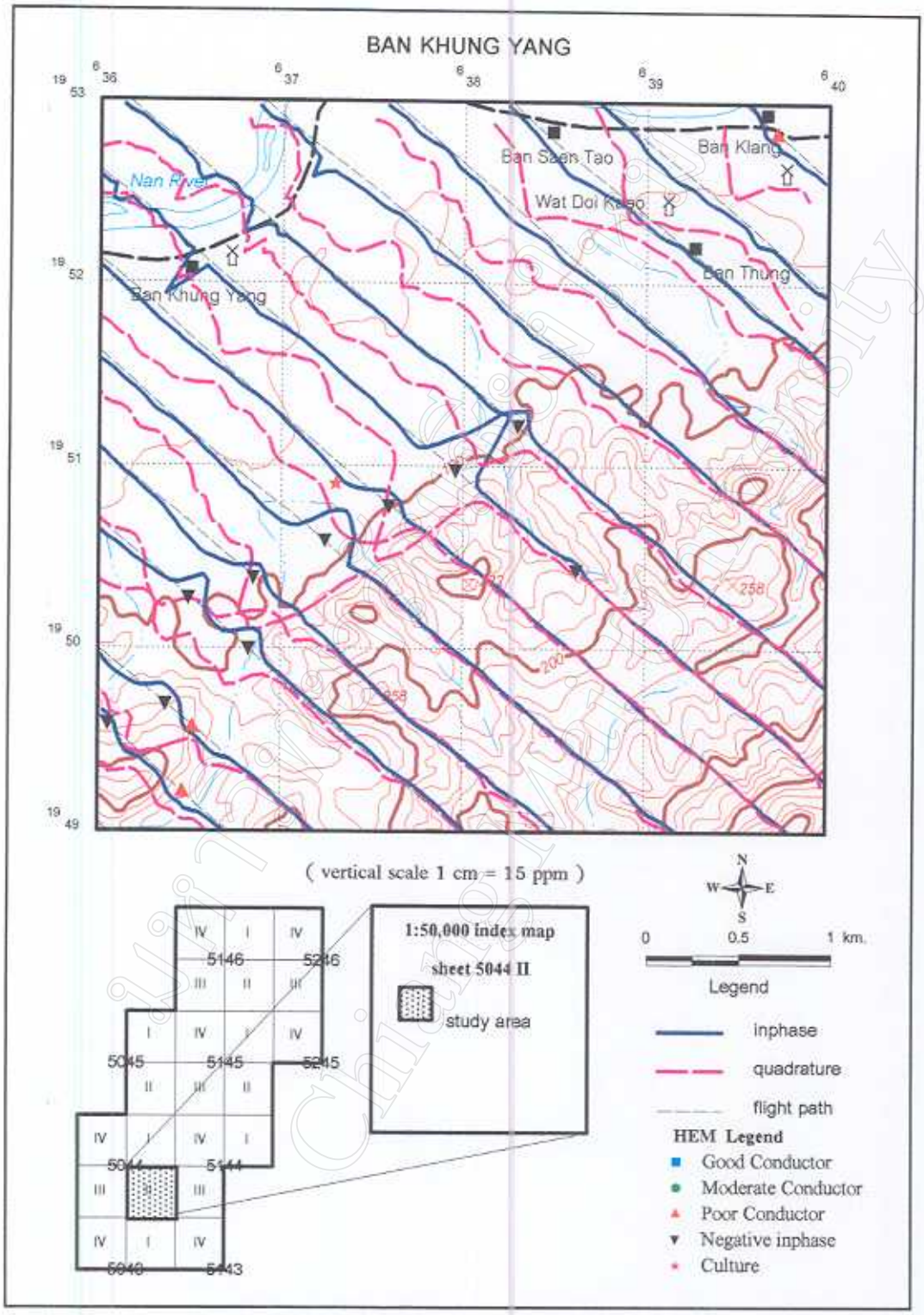

Figure 3.28 Helicopter-borne electromagnetic stacked profile over magnetic associated conductors.

3.2 Interpretation for regional geological framework

3.2.1 Regional framework of the northern part

In the northern area, there are two distinct geophysical anomalous zones. The west zone is composed of high radiometric response associated with circular magnetic anomaly (Figure 3.29a). On the other hand, the east zone is composed of non-radiometric part associated with an elongated magnetic anomaly. The radiometric anomaly in the west zone is impressive and forms an elongated feature that can be correlated with the Mesozoic volcanic (Mzv) units along the westernmost part of this area (Figure 3.29b). It is indicated that the Mzv is not composed of homogeneous radiometric material, or weathering products are different from place to place. Moreover, the circular magnetic zones found in this part cannot be related to any surface expression. More detailed study is needed to explain whether they indicate the conduit of eruption for the Mzv. To the west of this association, where Qt and Qa are the major outcrops, there is neither magnetic or radiometric anomaly. This indicates that the sediments constituting Qt and Qa are not derived from acidic igneous rocks where radioactive mineral is not prominent. Alternatively, these Qt and Qa areas may have high water content so that no radiation can penetrate.

There are two associations of high magnetic anomaly with low radiometric response in the eastern part of this area (Figure 3.29a) indicating the ultramafic units (Figure 3.29b). Although there are at least four ultramafic (U unit) mapped units, only two association zones are recognized. Therefore, the three ultramafic mapped units in the northern part must be connected at depth and more out crop should be found toward the east of the mapped ones. The northernmost mapped U unit (Figure 3.29b) is a thin slab compared to the other mapped U units because its expression does not continue vertically. In the south the U units are outcropping east of their centers marked by the magnetic anomaly (Figure 3.29a). The outcrops of these U units correlate very well with low radiometric zones and a more widespread distribution is expected. Unfortunately, there is no airborne geophysical data over the Cretaceous granite (Kgr) located at the southeastern part of this area (Figure 3.29b), where high radiometric anomaly associated with circular magnetic body is expected.

3.2.2 Regional framework of the central part

The associations of high radiometric and circular magnetic anomaly do not extend southward to this area (Figure 3.30a). On contrary, there is a distinct circular magnetic body with an unimpressive radiometric association toward the south. It also appears that the Triassic granite (Trgr) units found in the southwest

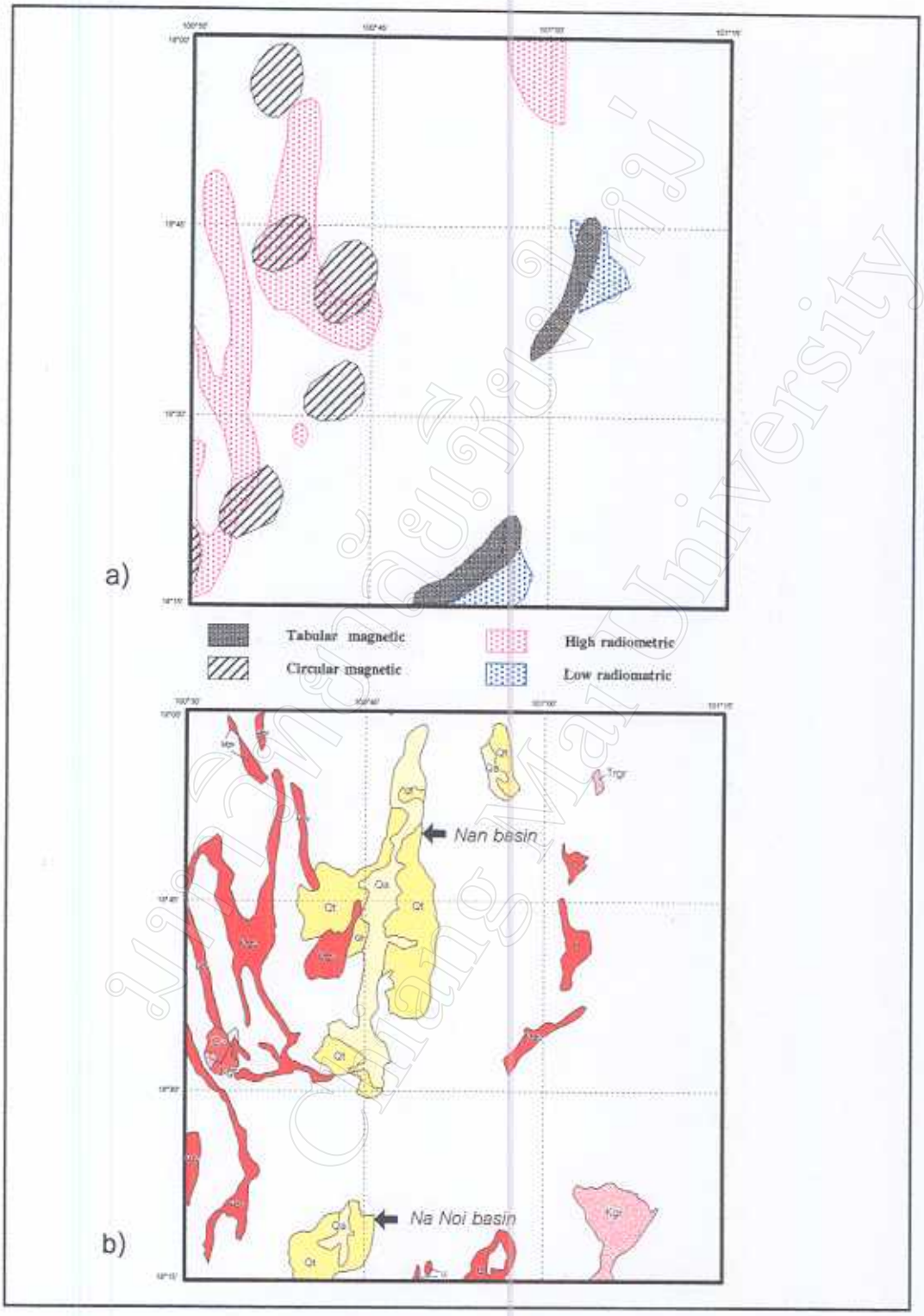

Figure 3.29 Regional geology (b) correlated with airborne geophysical data (a) in the northern part.
(symbols are the same as those in Figure 1.5)

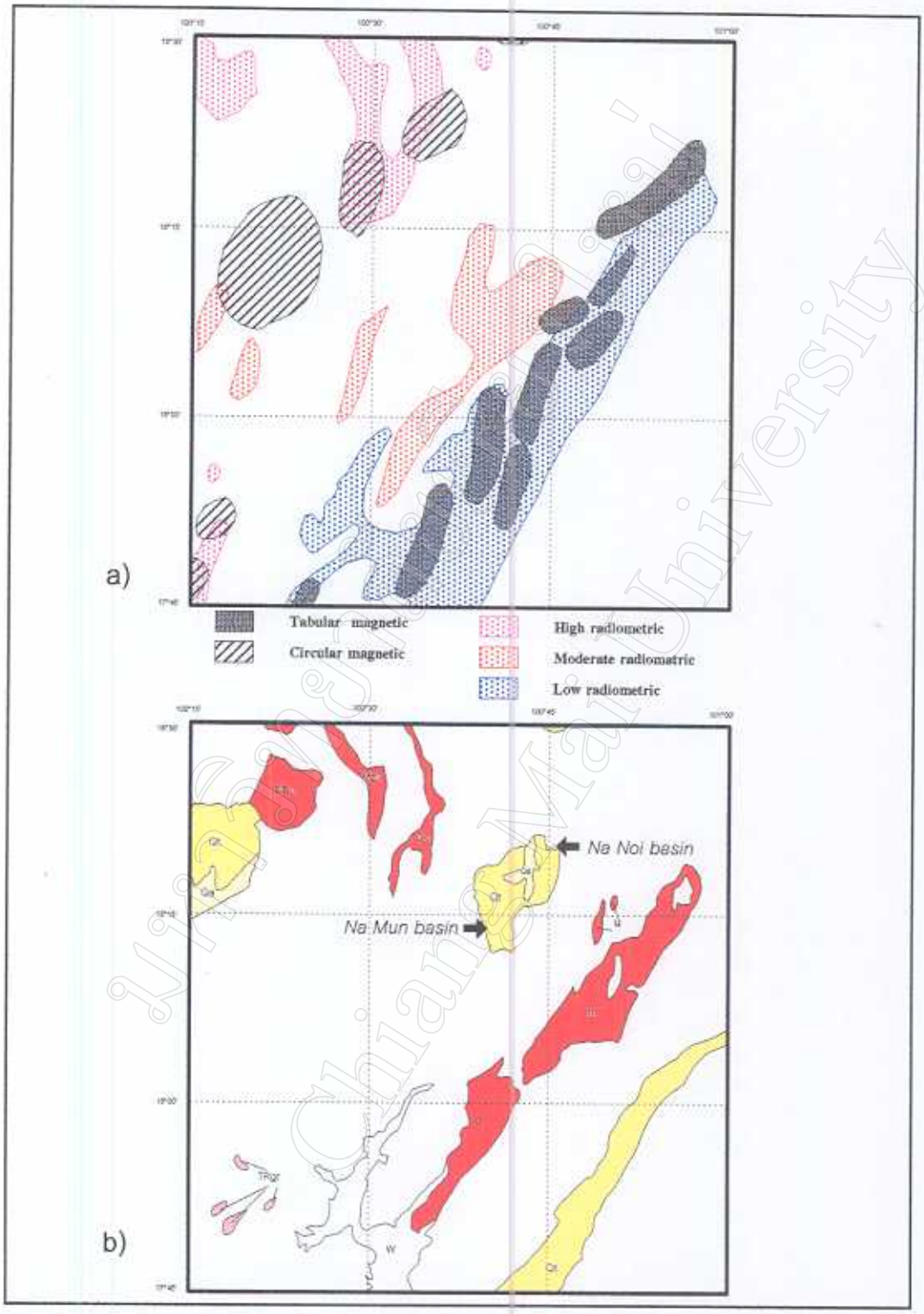

Figure 3.30 Regional geology (b) correlated with airborne geophysical data (a) in the central part.
(symbols are the same as those in Figure 1.6)

have no magnetic nor radiometric expression (Figure 3.30b), except the southernmost ones suggesting that there is no major intrusive body in that area and those granite units are not roof pendant. However, the associations of high magnetic anomaly with low radiometric response are the major expressions in the eastern half of this area. This indicates that the U units in this area are more widespread.

The magnetic data interpretation indicates that the U units are actually composed of many separated blocks, partly exposed as they are mapped. It should be noted here that part of the low radiometric areas is the water reservoir where radioactivity cannot be detected (Figure 3.30b). There is also a medium intensity radiometric zones west of the U units but no correlation with the mapped rock units can be made (Figure 3.30a).

3.2.3 Regional framework of the southern part

In this southern area, there are many interesting features drawn from airborne geophysical interpretations. More magnetic slabs are interpreted from aeromagnetic data but not high radiometric impression (Figure 3.31a). The continuation of magnetic slab that can be referred to the U unit extends toward the southwest underneath the Qt and Qa areas (Figure 3.31b). This indicates that the ultramafic units extend southward and more outcrops should be outlined where low radiometric response associated with magnetic slab locations. Moreover, the magnetic associated conductors, defined by negative inphase of HEM as mentioned earlier, are also interpreted as altered ultramafic rocks. The outcrop of ultramafic unit found outside the area of the mapped zone north of Ban Nam Phi is a good indicator for this interpretation (Figure 3.32a and Figure 3.32b).

There are two places that the association of high radiometric and high magnetic anomalies are found. The west one is correlated with an isolated granite stock close to a pair of the Mzv (Figure 3.31a and Figure 3.31b). The Mzv units are also indicated by high radiometric anomaly, and more Mzv units should be located toward the north of these mapped units. However, the other Mzv units in the south (Figure 3.31b) are not correlated with any radiometric anomalies (Figure 3.31a) even though they are more widespread. These may indicate that all southern Mzv units do not contain radiometric minerals or they were not precisely mapped due to thick overburden. The composition of these southern Mzv units is definitely different from the northwest one, therefore they must be separated in detailed mapping.

Another association of high radiometric and high magnetic anomalies, is located in the east of this area, both with circular features (Figure 3.31a) and without rock unit to be correlated (Figure 3.31b). Subsequent ground check made

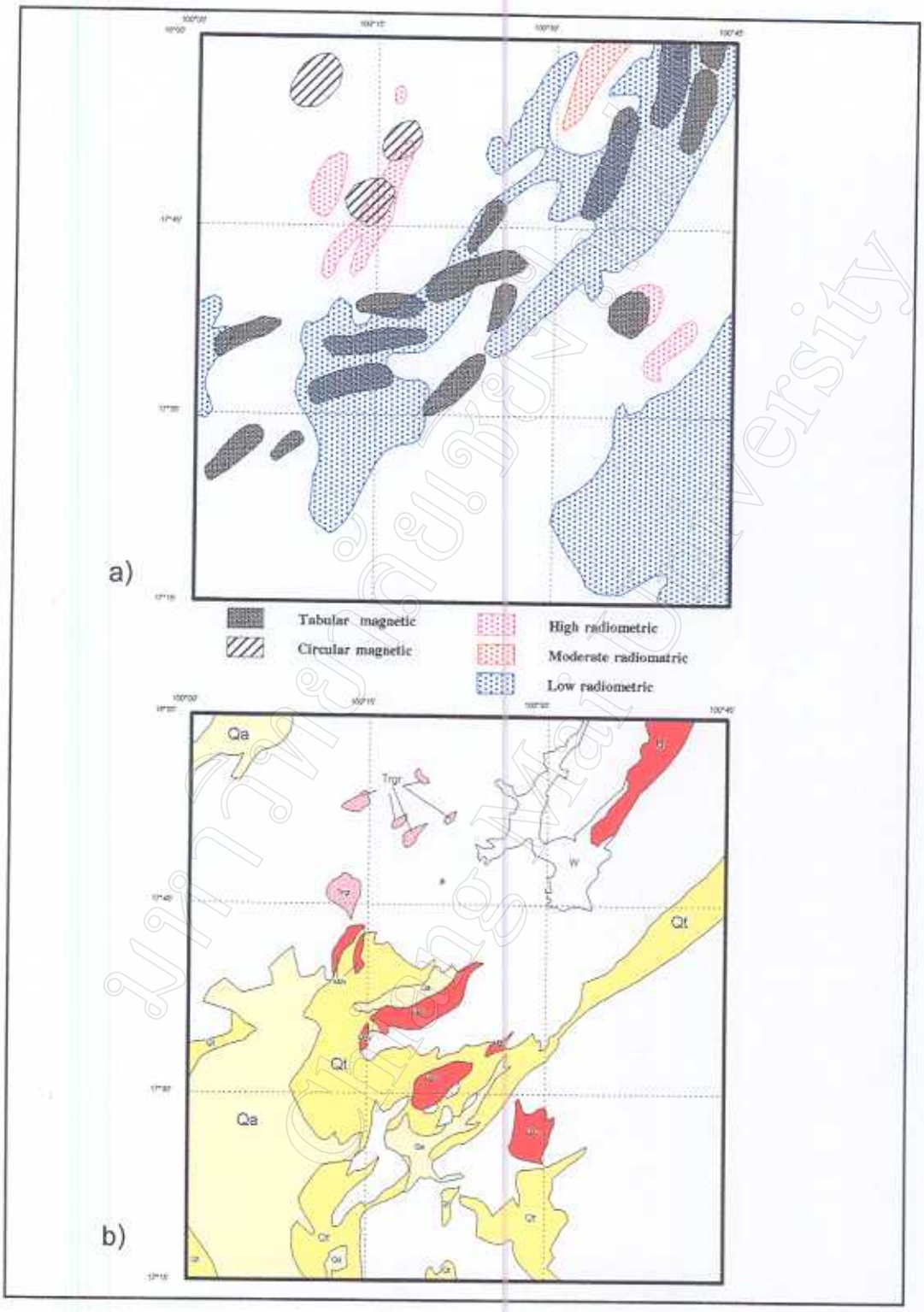

Figure 3.31 Regional geology (b) correlated with airborne geophysical data (a) in the southern part.
(symbols are the same as those in Figure 1.7)

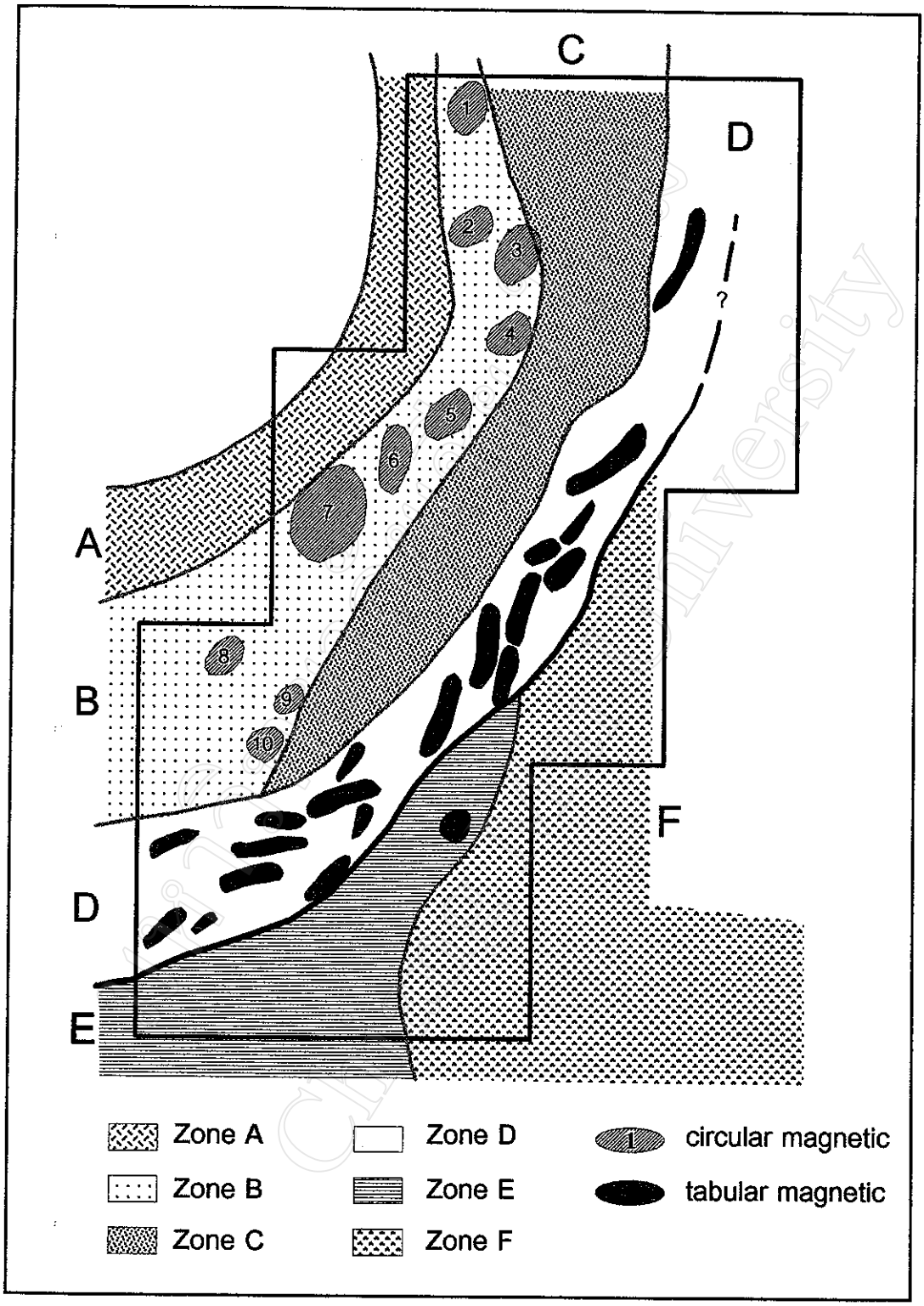

Figure 3.32 Tectonic framework of the study area interpreted from airborne geophysical data interpretation.

later found that there are loose blocks of altered sandstone and loosed block of rhyolitic porphyry in the vicinity of this association. The alteration may be hydrothermal resulted from some intrusive underneath.

3.3 Tectonic implications

The structural map of the NUS is presented in Figure 3.32. This map shows structure of magnetic and radiometric sources derived from the geological modelling interpretation made earlier. The structural map does not perfectly match the existing geological map. This is because attention was concentrated on all factors that might have an influence upon those physical properties. The map can be divided into two parts, marked by the heavy boundary line. This line is proposed to be the subduction zone, located between two different geophysical anomalous zones. To the west and north of this boundary line, there are four structural zones: Zone A, Zone B, Zone C, and Zone D, from the west to the east respectively. In the southeast, two structural zones: Zone E and Zone F are recognized.

No area in Zone A is characterized by distinct magnetic anomalous response. However, the radiometric anomaly is distinctive and appears as an elongated zone. This elongated zone is referred to the Mzv units. This zone may be covered by sedimentary sequence without any major intrusion.

Zone B and Zone C are difficult to be distinguished from each other solely by radiometric response. Zone B is composed of many isolated circular magnetic bodies and some elongated narrow zones. The volcanic rocks west of Nan basin are parts of this Zone B and extend toward the south to the volcanic rocks exposed at Ban Lao Pa Sa north of Uttaradit town center. No magnetic anomalous area, where sedimentary sequence and younger basin are mapped, characterizes Zone C. Basin boundary cannot be drawn from airborne geophysical data analysis, so ground check is required if detailed basin tectonic is needed. This Zone C extends from Nan basin through Na Noi basin to Na Mun basin. Its southern extension is located just north of Tha Pla District of Uttaradit.

Terrain in Zone D is a high mountain range where most of the rocks are characterized by melange. Magnetic anomalies are complex with superimposition of many tabular bodies. Dislocation and circular anomalies, with a minor extent, are present. The magnetic modelling shows that there are many slabs of ultramafic rocks thrusted over each other. Therefore, a multiple thrust of oceanic crust is represented by elongated ultramafic units lie almost parallel to each other. Northwestward dipping is also observed from their orientations. The model studies show that the depth of the buried slabs increases westward. Moreover, the radiometric data shows that more ultramafic outcrops should be outlined in this Zone D, and specific zone of melange can be more clearly defined.

To the east of the proposed subduction line, both Zone E and Zone F are outlined. Generally low radiometric intensities characterize the two zones but magnetic anomalies are located only in Zone E. Two types of magnetic anomalies are found: circular and superficial types. Superficial types are scattered throughout the zone but only one circular type is present in Zone E (Figure 3.32). The superficial magnetic features cannot be correlated with the mapped rock units in the regional scale but evidence of ultramafic rock extension and some volcanic activities are reported (e.g. Sukvattananunt and Prasittikarnkul, 1985).

The general tectonic setting of this study is based on the physical properties that referred to geological information. Therefore, definitions of each framework are drawn from interpretation of airborne geophysical survey data and ground verification is required. It can be concluded that effects of suturing evolution control the various features observed in this study area. Multiple thrusting events are observed from superimposed ultramafic units at depth. Westward dipping is concluded from magnetic modelling which also suggests that during collision the west block slid slightly toward the north. The ultramafic units were also thrusted over the younger units and more shallow buried ultramafic units are expected near the mapped ones. Minerals formed by segregation, chromite and nickel sulphide, are located within these ultramafic units. Figure 3.33 shows that there are three ultramafic units, marked by HEM stacked profiles, locate north of the Sirikit reservoir.

During suturing the ultramafic units were metamorphosed and parts of them are favourable places for hydrated minerals such as talc and chrysotile asbestos. Igneous activities took place mostly in the west block generally with associated hydrothermal alteration. Hydrothermal alterations produced many mineralization types and are located not far from the center of igneous activities outlined by integrated airborne geophysical survey data. However, the Khao Yai granite found southeast of Uttaradit (Sukvattananunt and Prasittikarnkul, 1985) shows a low alteration effect indicated by low radiometric anomalies (Figure 3.23a). Low conductance is also observed over the Khao Yai granite as indicated by low electromagnetic responses less than 2ppm on both inphase and quadrature components, in HEM stacked profiles (Figure 3.34).

After collision, the entire area is uplifted and weathering started to activate changing of minerals. Lateritic nickel was formed by residual concentration of ultramafic rocks in a high land while nickel chrome iron was formed in the low land. These minerals are principal targets, and ground geophysical survey will be applied in various environments mentioned above in order to make an economic evaluation.

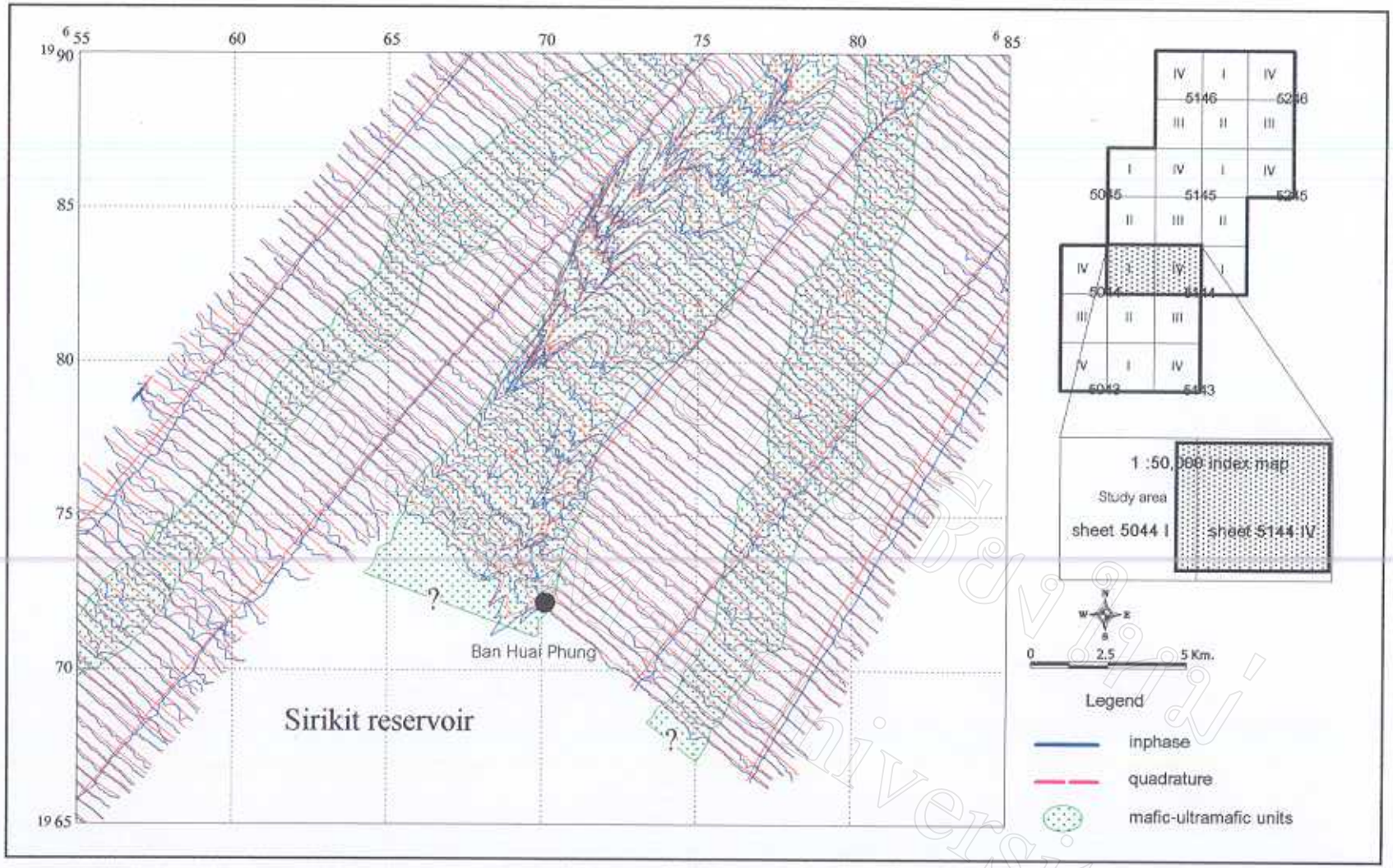

Figure 3.33 Map showing series of mafic-ultramafic blocks north of the Sirikit dam.

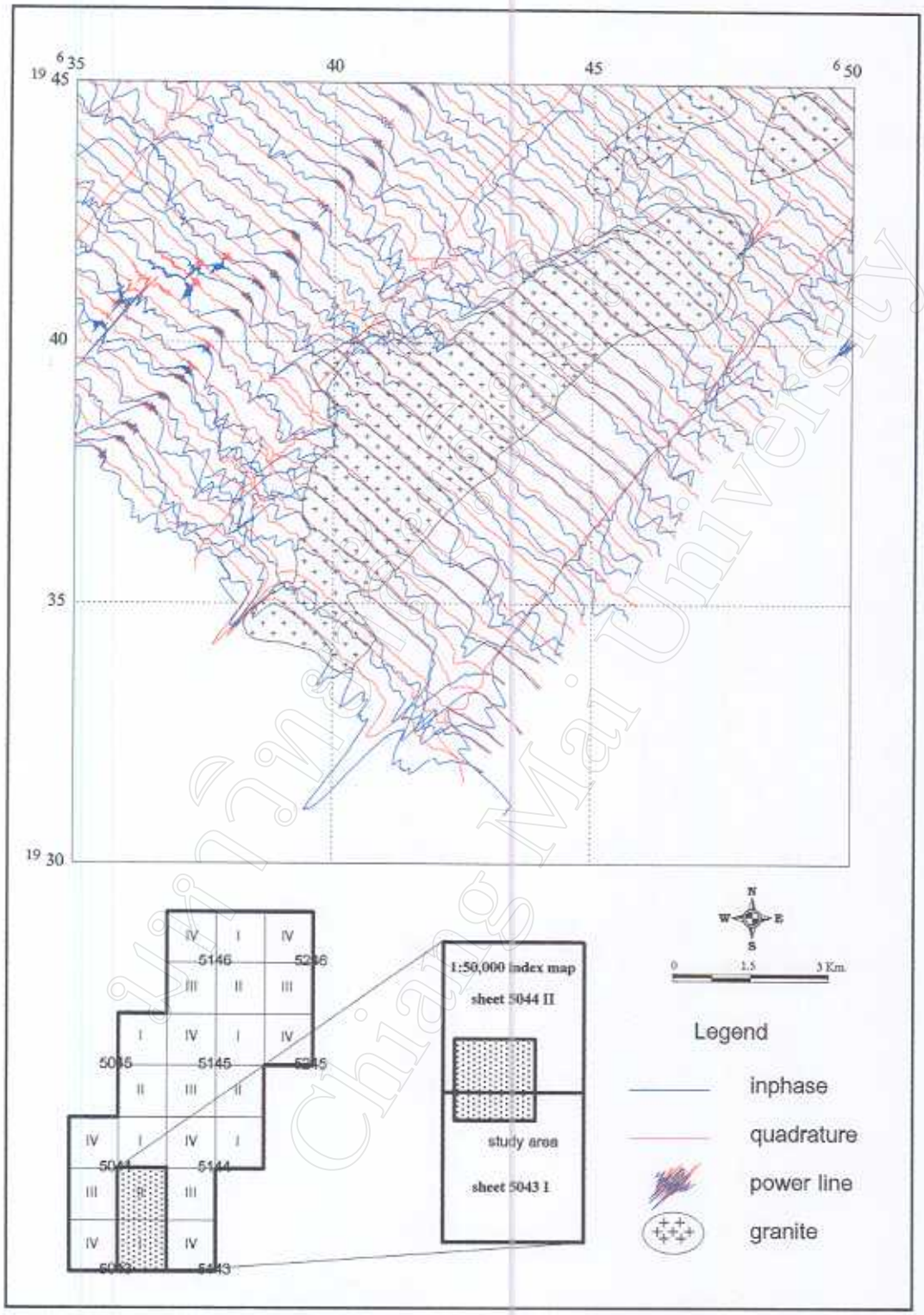

Figure 3.34 Map showing HEM stacked profiles over the Khao Yai granite.